(12) LEVEL II AD-E300 477

DNA 4513F

BLAST INDUCED DISTORTION EXPERIMENTS ON AN ENGINE INLET

Calspan Corporation
P.O. Box 400
Buffalo, New York 14225

30 January 1978

Final Report for Period February 1977—January 1978

CONTRACT No. DNA 001-77-C-0097

APPROVED FOR PUBLIC RELEASE;
DISTRIBUTION UNLIMITED.

THIS WORK SPONSORED BY THE DEFENSE NUCLEAR AGENCY
UNDER RDT&E RMSS CODE B342C77464 N99QAXAE50404 H2590D.

Prepared for
Director
DEFENSE NUCLEAR AGENCY
Washington, D. C. 20305

Destroy this report when it is no longer needed. Do not return to sender.

PLEASE NOTIFY THE DEFENSE NUCLEAR AGENCY, ATTN: TISI, WASHINGTON, D.C. 20305, IF YOUR ADDRESS IS INCORRECT, IF YOU WISH TO BE DELETED FROM THE DISTRIBUTION LIST, OR IF THE ADDRESSEE IS NO LONGER EMPLOYED BY YOUR ORGANIZATION.

UNCLASSIFIED

SECURITY CLASSIFICATION OF THIS PAGE (When Data Entered)

(17) REPORT DOCUMENTATION PAGE	READ INSTRUCTIONS BEFORE COMPLETING FORM
1. REPORT NUMBER: DNA 4513F, AD-E3pp 477	2. GOVT ACCESSION NO. (18) DNA, SBIE	3. RECIPIENT'S CATALOG NUMBER
4. TITLE (and Subtitle): (6) BLAST INDUCED DISTORTION EXPERIMENTS ON AN ENGINE INLET.	(9) 5. TYPE OF REPORT & PERIOD COVERED: Final Report for Period Feb 77—Jan 78
	6. PERFORMING ORG. REPORT NUMBER
7. AUTHOR(s): (10) Albert O. Davis, Michael G. Dunn	(15) 8. CONTRACT OR GRANT NUMBER(s): DNA 001-77-C-0097
9. PERFORMING ORGANIZATION NAME AND ADDRESS: Calspan Corporation, P.O. Box 400, Buffalo, New York 14225	(16) 10. PROGRAM ELEMENT, PROJECT, TASK AREA & WORK UNIT NUMBERS: NWED Subtask N99QAXAE504-04, (17) E 504
11. CONTROLLING OFFICE NAME AND ADDRESS: Director, Defense Nuclear Agency, Washington, D.C. 20305 (12) 72p.	(11) 12. REPORT DATE: 30 Jan 78; 13. NUMBER OF PAGES: 72
14. MONITORING AGENCY NAME & ADDRESS (if different from Controlling Office)	15. SECURITY CLASS (of this report): UNCLASSIFIED; 15a. DECLASSIFICATION DOWNGRADING SCHEDULE

16. DISTRIBUTION STATEMENT (of this Report)

Approved for public release; distribution unlimited.

17. DISTRIBUTION STATEMENT (of the abstract entered in Block 20, if different from Report)

18. SUPPLEMENTARY NOTES

This work sponsored by the Defense Nuclear Agency under RDT&E RMSS Code B342077464 N99QAXAE50404 H2590D.

19. KEY WORDS (Continue on reverse side if necessary and identify by block number)

Inlet Distortion
B-1 0.1 Scale Model
Shockwave/Boundary-Layer Interaction

20. ABSTRACT (Continue on reverse side if necessary and identify by block number)

This report briefly reviews the results of the Kaman AviDyne/AEDC experimental program funded by DNA. The purpose of this program was to develop an experimental technique that could be used to define the nuclear-blast-induced distortion at the inlet/engine interface of aircraft and air-breathing missiles. The result of the test program have been evaluated as has the potential impact of these results on other air-breathing engines with inlets having different L/D values.

DD FORM 1 JAN 73 1473 EDITION OF 1 NOV 65 IS OBSOLETE

UNCLASSIFIED

SECURITY CLASSIFICATION OF THIS PAGE (When Data Entered)

40 727

TABLE OF CONTENTS

Section		Page
	LIST OF ILLUSTRATIONS	2
1	INTRODUCTION	5
2	EFFECTS OF BLAST WAVES ON AIRBREATHING PROPULSION SYSTEMS	7
3	FACTORS AFFECTING PROPULSION-SYSTEM BLAST TOLERANCE AND SIGNIFICANCE	8
4	BRIEF SUMMARY OF KAMAN/AEDC TEST PROGRAM	11
	4-1 INLET MODEL	11
	4-1.1 Model Instrumentation	13
	4-1.2 Dynamic Pressure Transducers and Calibration	13
	4-1.3 Data Acquisition and Reduction	13
5	DISCUSSION OF RESULTS	16
	5-1 INCIDENT SHOCK-WAVE INTERACTION WITH B-1 INLET	16
	5-1.1 Claw-Probe Data	18
	5-1.2 Inlet Duct Pressure Measurements	20
	5-1.3 Aerodynamic Interface Plane Total-Pressure Measurements	27
	5-1.4 Distortion Data	36
	5-2 COMPARISON WITH PREVIOUS DISTORTION DATA	42
	5-3 DISTORTION TEST RESULTS	45
	5-3.1 Distortion Methodology and Inlet/Engine Compatibility	45
	5-3.2 AEDC Wind Tunnel Test Results for Δp of 2.0 and 2.5 psi	48
	5-4 COMPARISON WITH FLIGHT TEST DATA	58
6	CONCLUSIONS	65
7	RECOMMENDATIONS	66
	REFERENCES	67

LIST OF ILLUSTRATIONS

Figure		Page
1	Typical Compressor Stall Map	9
2	Inlet Area Distribution (Full Scale)	12
3	Inlet Static Pressure Locations for Dynamic Measurements	14
4	Top View of Test Installation in AEDC 16T Tunnel	17
5	Claw Probe Total Pressure Ratios and Typical M_o = 0.85 Part 546 Tube No. 1	19
6	Comparison of Qualitative Characteristics of Claw Probe Static Pressure and Duct Static Pressure Histories for Shock Tube No. 1	21
7	Comparison of Qualitative Characteristics of Claw Probe Static Pressure and Duct Static Pressure Histories for Shock Tube No. 2	23
8	Inlet Cowl Surface Static Pressure Ratios Across the Incident Shock M_o = 0.85 Part 546 Tube No. 1	26
9	(a) Outboard Inlet AIP Total Pressure Ratio Across the Incident Shock M_o = 0.85 Part 546 Tube No. 1	28
	(b) Outboard Inlet AIP Total Pressure Ratio Across the Incident Shock M_o = 0.85 Part 546 Tube No. 1	29
	(c) Outboard Inlet AIP Total Pressure Ratio Across the Incident Shock M_o = 0.85 Part 546 Tube No. 1	30
	(d) Outboard Inlet AIP Total Pressure Ratio Across the Incident Shock M_o = 0.85 Part 546 Tube No. 1	31
	(e) Outboard Inlet AIP Total Pressure Ratio Across the Incident Shock M_o = 0.85 Part 546 Tube No. 1	32
	(f) Outboard Inlet AIP Total Pressure Ratio Across the Incident Shock M_o = 0.85 Part 546 Tube No. 1	33
	(g) Outboard Inlet AIP Total Pressure Ratio Across the Incident Shock M_o = 0.85 Part 546 Tube No. 1	34
	(h) Outboard Inlet AIP Total Pressure Ratio Across the Incident Shock M_o = 0.85 Part 546 Tube No. 1	35

Figure		Page
10	(a) Inboard Inlet AIP Total Pressure Ratio Across the Incident Shock M_o = 0.85 Part 546 Tube No. 1	37
	(b) Inboard Inlet AIP Total Pressure Ratio Across the Incident Shock M_o = 0.85 Part 546 Tube No. 1	38
11	Average AIP Total Pressure Recovery M_o = 0.85 Part 546 Tube No. 1	39
12	(a) Outboard Inlet Distortion Indices M_o = 0.85 Part 546 Tube No. 1	40
	(b) Inboard Inlet Distortion Indices M_o = 0.85 Part 546 Tube No. 1	41
13	(a) Model Scale Effect on Distortion	43
	(b) Model Scale Effect on Stall Margin Index	44
14	Summary of Reynolds Number and Scale Effects	46
15	Digital Stall Margin Ratio Versus Time, Filtered to Various Frequency Levels	49
16	Influence of Time Averaging on Stall Margin Index	50
17	Influence of Frequency on Stall Margin Index	51
18	Average AIP Total Pressure Ratio Behind Pressure Disturbance	53
19	(a) Influence of Air Flow on Stall Margin Index	54
	(b) Influence of Yaw Angle on Stall Margin Index	55
	(c) Effect of Incident Shock Upon Stall Margin Index	56
	(d) Typical Distortion Values at M = 0.9	57
20	(a) Steady-State Inlet Flight Performance	60
	(b) Steady-State Inlet Flight Performance	61
21	(a) Outboard Inlet AIP Steady-State Total Pressure Contours Mach No = 0.7, Flight 2-23	62
	(b) Outboard Inlet AIP Dynamic Total Pressure Contours Mach No. = 0.7, Flight 2-23	63

SECTION 1

INTRODUCTION

Nuclear survivability/vulnerability (S/V) has been a consideration for several years in the design of strategic aircraft and missile systems. Typically, assessments of such systems have included determination of the structural blast response (using computer codes such as NOVA and VIBRA), structural examination of the blast-induced aerodynamic gust response, evaluation of the structural thermal-pulse response, and investigation of transient radiation effects and electromagnetic pulse on electronics. In more recent years, the need to extend nuclear S/V assessments to aircraft and missile propulsion systems has been recognized. Only the B-1 (S/V) assessment dealt with the propulsion system, but it could not treat the problem in detail because the methodology to do so was not well developed.

A nuclear blast wave has associated with it a nearly step-function pressure and temperature pulse to which an operating propulsion system may be subjected. The response of the propulsion system and associated potential problems is recognized as an important consideration that must be treated in nuclear S/V studies of systems utilizing airbreathing engines. Because this is a relatively new aspect of nuclear S/V response, it is one for which only limited theoretical work has been done. Even less work has been done with the very small amount of applicable experimental data, with the result that at present an established methodology is not available for assessing the blast response of airbreathing propulsion systems.

As a result of this significant technology void, the Defense Nuclear Agency (DNA) contracted with Kaman AviDyne and the Arnold Engineering Development Center (AEDC) with the purpose of developing an experimental technique that could be used to define the nuclear-blast-induced distortion at the inlet/engine interface of aircraft and airbreathing missiles. As part of this program, the 0.1 scale B-1 inlet model was installed in the AEDC 16-T facility and subjected to simulated blast waves at selected overpressures. The B-1 inlet model was used because it was an existing well-instrumented, previously tested model that was made available to DNA by the B-1 SPO and because it would serve the purposes of the developmental program.

A description of the AEDC experimental apparatus, the test-condition matrix, and a discussion of the data analysis procedures and results can be found in the Kaman AviDyne report (Reference 1) of this program. Calspan's purpose in this program was to serve as an advisor to DNA, to evaluate briefly the results of the test program discussed above, and to assess the potential impact of those results on other airbreathing engines with inlets having different L/D values. As part of this limited effort, we reviewed in detail the data from 18 selected tests out of the approximately 43 tests performed.

SECTION 2

EFFECTS OF BLAST WAVES ON AIRBREATHING PROPULSION SYSTEMS

In assessing the response of a given airbreathing propulsion system to blast waves, the two primary mechanisms that must be considered are the distorted inlet flow and the engine response to internal waves. In the first, the blast wave, in the process of diffracting about the nacelle and propagating down the inlet, produces a distorted inlet flow. If the distortion is sufficiently severe then engine stall, surge, flameout, or damage may result. The effect of blast waves on B-1 inlet-flow distortion has been examined experimentally under DNA funding as noted above. To Calspan's knowledge, the Kaman/AEDC experimental program is the first such attempt to study the behavior of an engine inlet in a simulated flight/blast environment. These data can now be used as a foundation for developing a predictive technique for inlet response to blast waves of various strengths. A further methodology is needed for relating the effects of the propagating blast front to the engine response within a transient framework. The Kaman/AEDC data are not sufficient for this latter task, but the Suffield (References 2-4) experimental data for a turbojet engine (Orenda 8) are a good starting point.

SECTION 3

FACTORS AFFECTING PROPULSION-SYSTEM BLAST TOLERANCE AND SIGNIFICANCE

The blast tolerance, including the relative importance of inlet-flow distortion and internal blast-wave propagation, is governed by many factors. The engine type is of obvious importance; turbojets, turbofans, ramjets, etc. will respond differently to any given blast environment. For any particular engine type, the detailed internal gasdynamic response will generally depend on the internal engine configuration (the number and type of compressor and turbine stages, combustor type, etc.), on the engine operating point (stage pressure and stall-margin ratios, nozzle pressure ratio, turbine inlet temperature, fuel/air ratio, etc.), and on the engine control system (measurement parameters, response characteristics, etc.). (Figure 1 is a typical plot of compressor pressure vs. mass-flow ratio illustrating the stall line and the normal operating line for various compressor rpm values. It is probable that the blast-wave-associated pressure pulse would move the stall line closer to the normal operating line with the engine speed remaining nearly constant on the time scale of interest.) The inlet type (internal, external, or mixed compression; high or low length-to-diameter ratio; boundary-layer bleed and bypass provisions; etc.) can strongly modify blast waves entering the engine from the front by changing the blast strength and introducing distortion. Finally, the nuclear-blast strength and orientation with respect to the weapon system will strongly affect the transient internal-engine pressures and temperatures that result.

The various factors cited above must be considered in determining whether a given blast wave will produce stall, surge, foreign object impingement, or flameout in any given case. It is possible for these conditions to occur without resultant engine damage. Whether physical damage occurs in any given case depends on engine component strength and materials.

The blast response of the propulsion system can affect mission survivability in a number of ways. If engine damage is produced such that engine operation ceases or results in a fire, the mission cannot be completed. It should be noted that the use of multiple engines does not necessarily improve mission survivability since it is possible that all engines could be affected similarly.

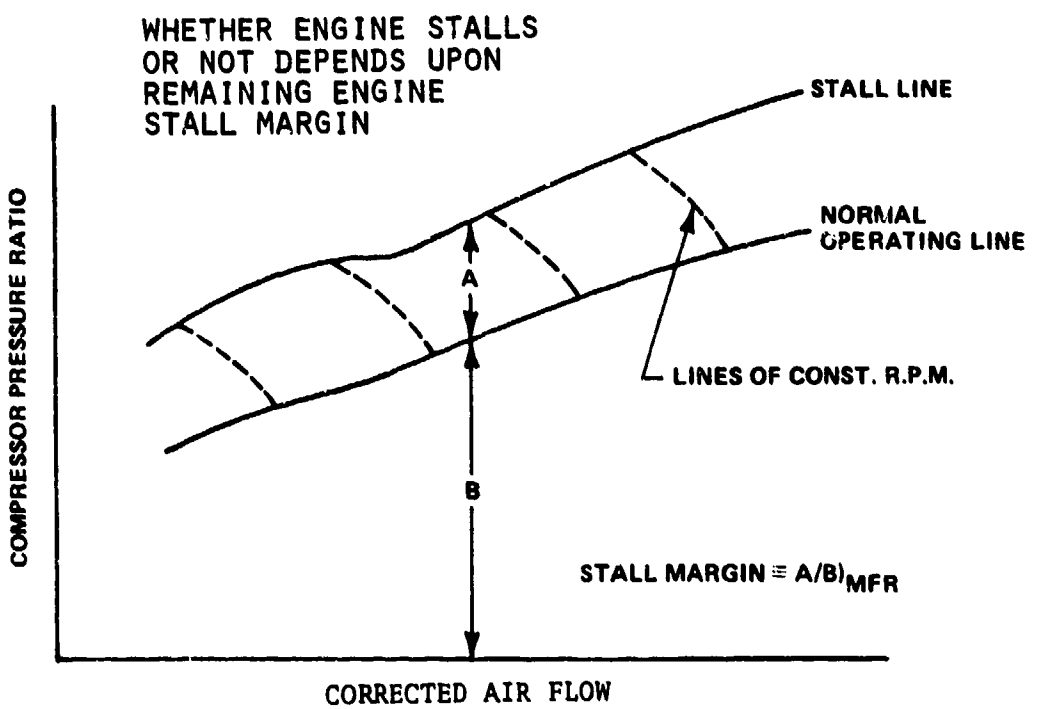

Figure 1 Typical Compressor Stall Map

If engine damage (e.g., compressor blade degradation) occurs, causing reduced performance but not preventing the engines from functioning, then mission survivability depends on the extent of the performance degradation.

Similarly, if no damage occurs but a flameout is produced, mission survivability depends on the restart capability provided. Even if restart capability is provided, a flameout could constitute mission kill under certain conditions. For example, if the mission involved low-altitude penetration, a flameout could be critical, depending on the engine restart time at the mission condition. In some systems, this time may be as high as one minute. In those cases, a flameout would be hazardous.

SECTION 4

BRIEF SUMMARY OF KAMAN/AEDC TEST PROGRAM

The primary emphasis in this and the following section will be placed on ascertaining the validity of the experimental results and on relating the distortion results to the B-1 inlet/engine system. The subject of inlet flow distortion and its effects on inlet/engine compatibility is an exceedingly difficult one. A distinction is usually made between steady-state and dynamic distortion, where steady-state distortion refers to steady spatial flow non-uniformities while dynamic distortion is a measure of inlet-flow turbulence. Dynamic distortion methodology is only about ten years old and therefore it was not considered in many recent weapons systems as noted in Section 1. Considerable progress has been made recently (References 5-7) towards developing methodologies for evaluating and quantifying the effects of steady-state and dynamic distortion.

4-1 INLET MODEL

The inlet model used by Kaman/AEDC represented the B-1 aircraft inlet internal lines to the aerodynamic interface plane (AIP). The external inlet lines were duplicated only in the vicinity of the cowl, sideplates and bypass doors. Each inlet was equipped with a variable ramp geometry, but for these measurements the ramps were rigidly fixed in the subsonic position. The model represented the B-1 aircraft forward fuselage and had a stub wing with a dual inlet left-hand nacelle. The stub wing represented the 67.5° sweep case. The right-hand stub wing was not simulated. A complete description of the model and associated instrumentation can be found in Reference 8.

The inlet area distribution as a function of full-scale nacelle station is given in Figure 2. The subsonic ramp settings, which were used in these experiments, correspond to the upper curve while the lower curve represents the supersonic cruise configuration.

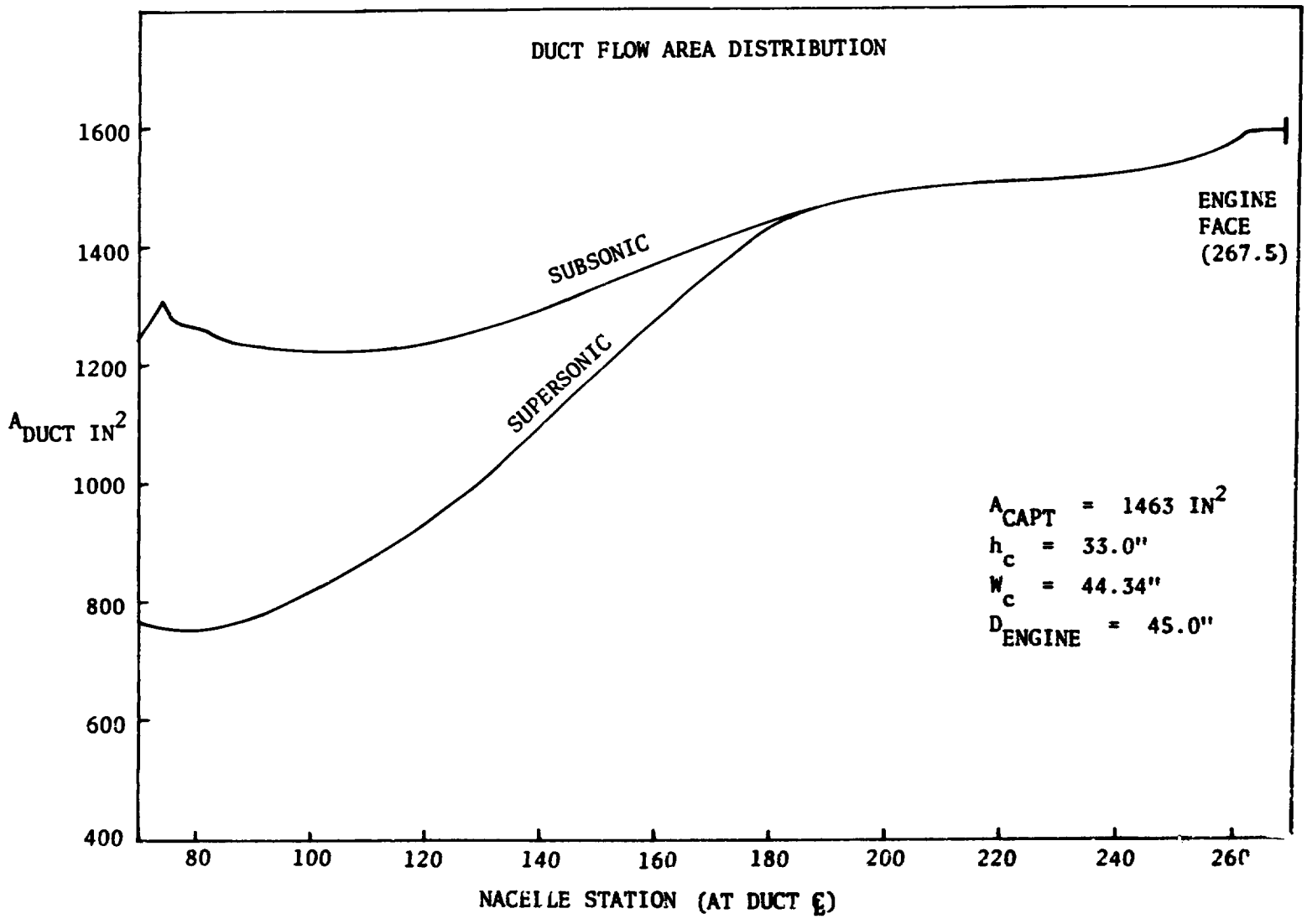

Figure 2 Inlet Area Distribution (Full Scale)

4-1.1 Model Instrumentation

References 1 and 9 contain a complete description of the model instrumentation and thus these details will not be repeated here. For the purposes of our discussion, only the dynamic-pressure data are relevant. Nine surface static-pressure measurements were taken in the outboard inlet and a single static-pressure transducer was located on the inner surface of the inboard inlet as shown on Figure 3. As will be discussed later, these measurements were used in an unsuccessful attempt to determine the blast-wave propagation characteristics along the inlet.

Each inlet had forty total-pressure probes located at the aerodynamic interface plane (AIP). The rake circumferential spacing corresponds to the location of the F101-GE-100 engine inlet guide vanes.

4-1.2 Dynamic Pressure Transducers and Calibrations

The dynamic-pressure transducers were Kulite CQL-080-25 differential type. The 16-T tunnel free-stream total pressure was used to reference all of the differential pressure transducers and to normalize the dynamic-pressure measurements. The transducers were calibrated by Rockwell (Reference 9) using a simple shock tube arrangement to produce a step pressure pulse of well known value. In addition, it was determined that an upper filter limit of 0.1 MHz provided the best compromise between rise time and transducer ringing. The basic transducer has a natural frequency of 125 KHz. The majority of the transducers had a response time of 25 μsec or less. These response times are felt to be sufficient to provide valid AIP blast-wave pressure data.

4-1.3 Data Acquisition and Reduction

The data acquisition and reduction procedure is discussed in detail by AEDC (Reference 10). The material presented here is a brief summary of that procedure provided for completeness.

The steady-state pressure data were recorded on the AEDC-16T precision pressure balance and the dynamic data were recorded unfiltered as analog counts

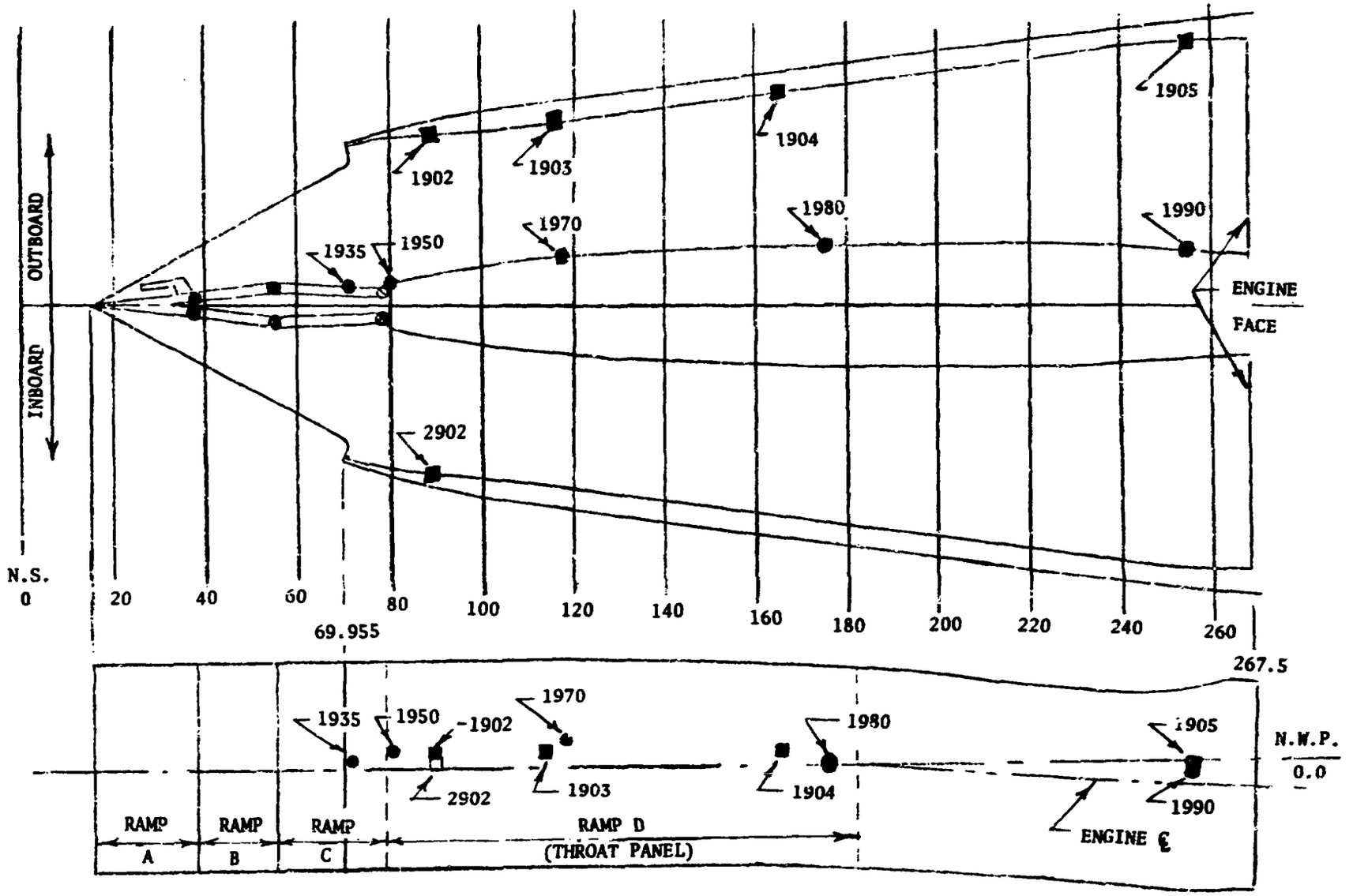

Figure 3 Inlet Static Pressure Orifice Locations for Dynamic Measurements

on a Vidar FM multiplex (VIDAR/MUX) tape unit recording at 240 inches per second. The analog data were then digitized at a playback speed of 7.5 inches/sec with a 1.0 KHz filter. Each channel was digitized at a time interval of approximately 10.452 μsec between samples. The data reduction scheme and the calculation of the various distortion parameters were consistent with the Rockwell procedure described in References 6, 11 and 12. Reduction procedure of the claw-probe data was prescribed by Kaman and is given in Reference 11.

SECTION 5

DISCUSSION OF RESULTS

Exploratory tests performed by Kaman AviDyne in the AEDC 1T wind tunnel suggested that shock-tube generated pressure pulses could be used to simulate blast waves in a transonic test facility. Other authors (References 13-19) have previously looked at the feasibility of simulating blast waves using shock tubes in wind tunnels/shock tunnels or other techniques. However, none of these previous authors had carried the problem to the final step of attempting to perform an engine inlet experiment.

Schlieren photographs obtained by Kaman/AEDC in the 1T experiments suggested that a quasi-spherical wave followed by a short-time interval of quiescent flow was generated. The quiescent flow was followed by an extremely turbulent region probably resulting from the shock-tube reflected wave action. On the basis of the encouraging 1T tests, three shock tubes were installed in the walls of the AEDC 16T facility and the Kaman experimental program was conducted. The details of these experiments, the physical layout, matrix of test conditions and data analysis will be given in detail in Reference 1 when that report becomes available. In the following pages of this report the validity of the test results and their application to inlet-distortion testing and interpretation of these results with respect to the B-1 propulsion system will be discussed. Conclusions of the test program are discussed and recommendations for additional work in this area are presented.

5-1 INCIDENT SHOCK-WAVE INTERACTION WITH B-1 INLET

The discussion in this and the following subsections will use Part 546 as an illustrative example. The test conditions correspond to a free-stream Mach number (M_o) of 0.85, corrected weight flow (W1R) of 350 lb/sec, and a nominal Δp of 2.0 psi from shock tube #1 (see Figure 4).

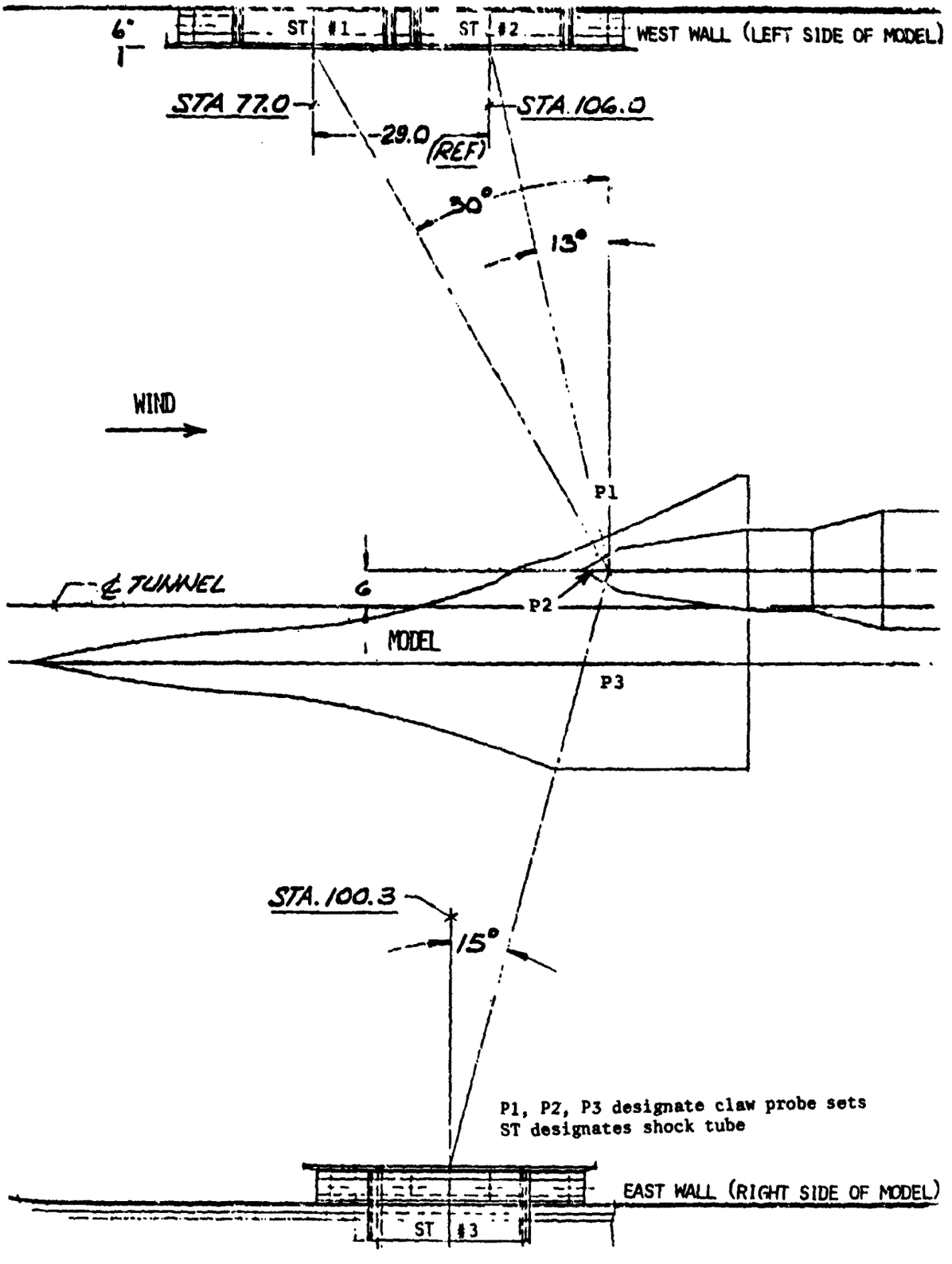

Figure 4 Top View of Test Installation in AEDC 16T Tunnel

5-1.1 Claw-Probe Data

For these experiments there were three claw-type probes (see Reference 20), located as shown in Figure 4, which were intended to provide an indication of the incident-wave arrival times, pressure levels, flow angularity, and flow quality. Typical claw-probe total-pressure traces are reproduced in Figure 5. Unfortunately, instrumentation problems appear to have limited the utility of these probes to the indication of the incident-wave arrival times, approximate overpressure ratio and an indication of the duration of valid test time for distortion analysis.

The claw probes consisted of two total-pressure and one static-pressure measurements. It is beyond the scope of this report to present detailed results from both the right- and left-hand total pressure probe measurements (see Reference 1), but the established trends will be discussed. In nearly all tests, either one or the other of the claw total-pressure measurements was suspect. In many cases, one probe was obviously not responding properly. In other cases where both probes appeared to have valid response, the leeward probe (defined as the left-hand probe for shock tubes numbers 1 and 2, and the right-hand probe for shock tube number 3) indicated pressure rises up to twice those obtained for the windward probe. Hence, one cannot average the data shown in Figure 5 and use it readily in detailed flow-field computations. The value of PTC1 given in Figure 5 is based on the left-hand probe only.

The results presented in Figure 5 were unexpected in that they indicate generally greater pressure ratios for probe 2 than were obtained for probe 1. It was anticipated that probe 2 pressure levels would be less than those of probe 1 because probe 2 was located at a greater distance from the shock-tube exit and thus the attenuation of the incident wave should have been greater and because diffraction over the nacelle would tend to lower the pressure. This behavior was seen in many of the tests suggesting that the absolute pressure levels obtained with the claw probes may be questionable.

The third claw probe is located on the leeward side of the nacelle for tests using shock tubes numbers 1 and 2. Reference to Figure 5 indicates considerable attenuation as would be expected. Examination of the probe 3 right- and left-hand total-pressure results indicated a flat-peak characteristic for either one or

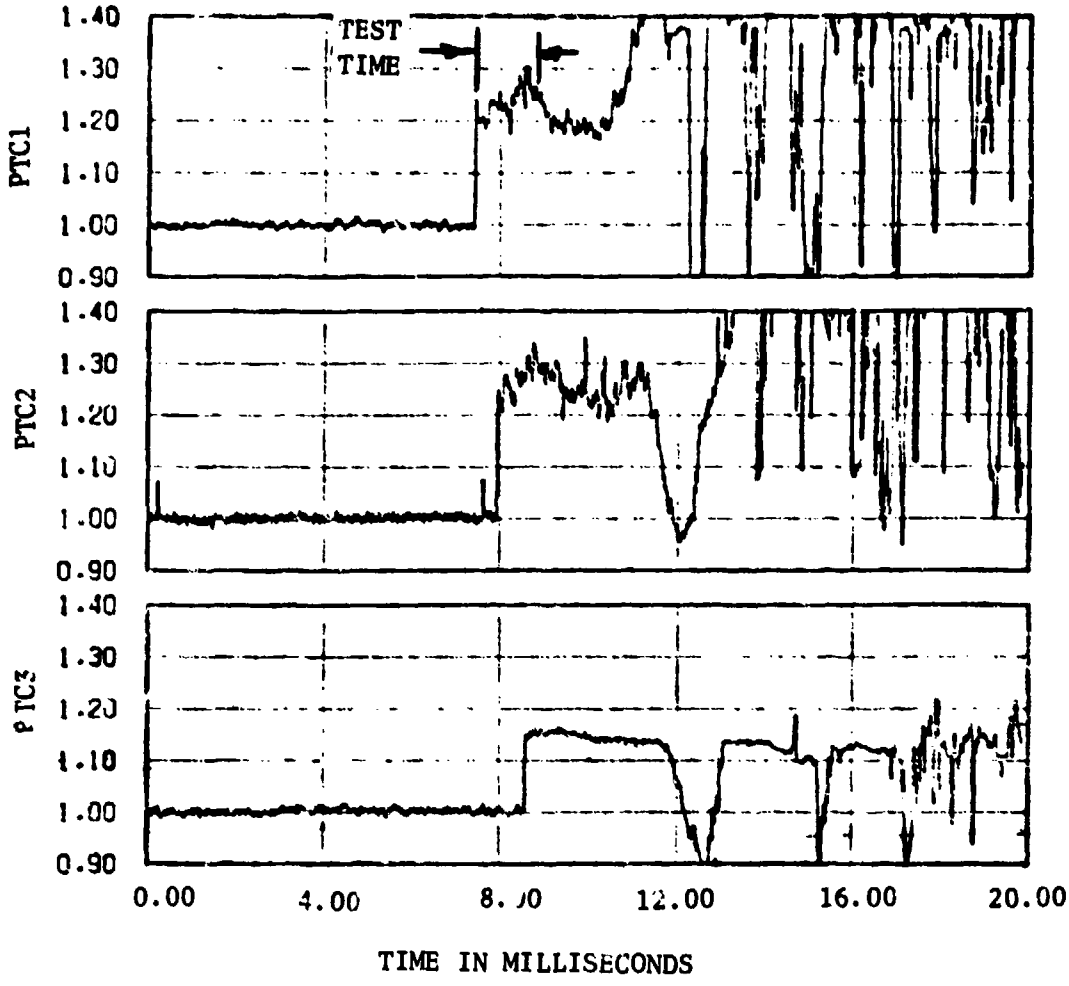

Figure 5 Claw Probe Total Pressure Ratios
M_o = 0.85 Part 546 Tube No. 1

both traces. This characteristic is indicative of a possible instrumentation gain cut-off. Analogous behavior was noted for tests involving shock tube number 3.

The claw probes did provide a good indicator of the extent of relatively uniform flow behind the incident shock. In Figure 5, an interval of approximately 1 millisecond is labelled test time for the claw-probe location. Ideal-gas calculations of the test time behind the incident shock near the end of the shock tube and prior to the shock-processed gas entering the 16T free-stream flow gave a test time on the order of 3.5 milliseconds. In the absence of considerable additional work, it is not unreasonable to assume that one might get a test time on the order of 1.0 millisecond at the claw probe location for these flow conditions. However, the proper calculation that should be performed is a coupled one that allows for the interaction between the shock-tube flow and the oncoming Mach number = 0.85 free-stream flow. It would not suffice to do the calculation for a quiescent free-stream flow.

The initial pressure spike seen in PTC 1 and PTC 2 records is believed to be ringing of the transducer, while it is not apparent whether the rise seen on PTC 1 from a value of 1.20 to 1.24 is a result of the transducer response or whether it is real. Further insight into the uniformity of this flow interval may be obtained by examining the claw probe 1 static pressure ratio, PS1 for Part 546, which is given as a portion of Figure 6 and is on the same time scale as Figure 5. The point of this comparison is that in general, the basic characteristics of the claw-probe static and total-pressure records were consistently similar. Also included on Figure 5 for comparison purposes is claw probe 3 total-pressure data which will be discussed later in terms of the leeward-side engine face total-pressure data.

5-1.2 Inlet Duct Pressure Measurements

Figures 6 and 7 present comparisons between the claw-probe 1 static pressure, PS1, and static-pressure transducer #1980 located in the inlet duct (see Figure 3 for location). The comparison between PS1 and #1980 results is presented for Mach numbers 0.55, 0.7, 0.85 and 0.90 for shock tubes numbers 1 and 2.

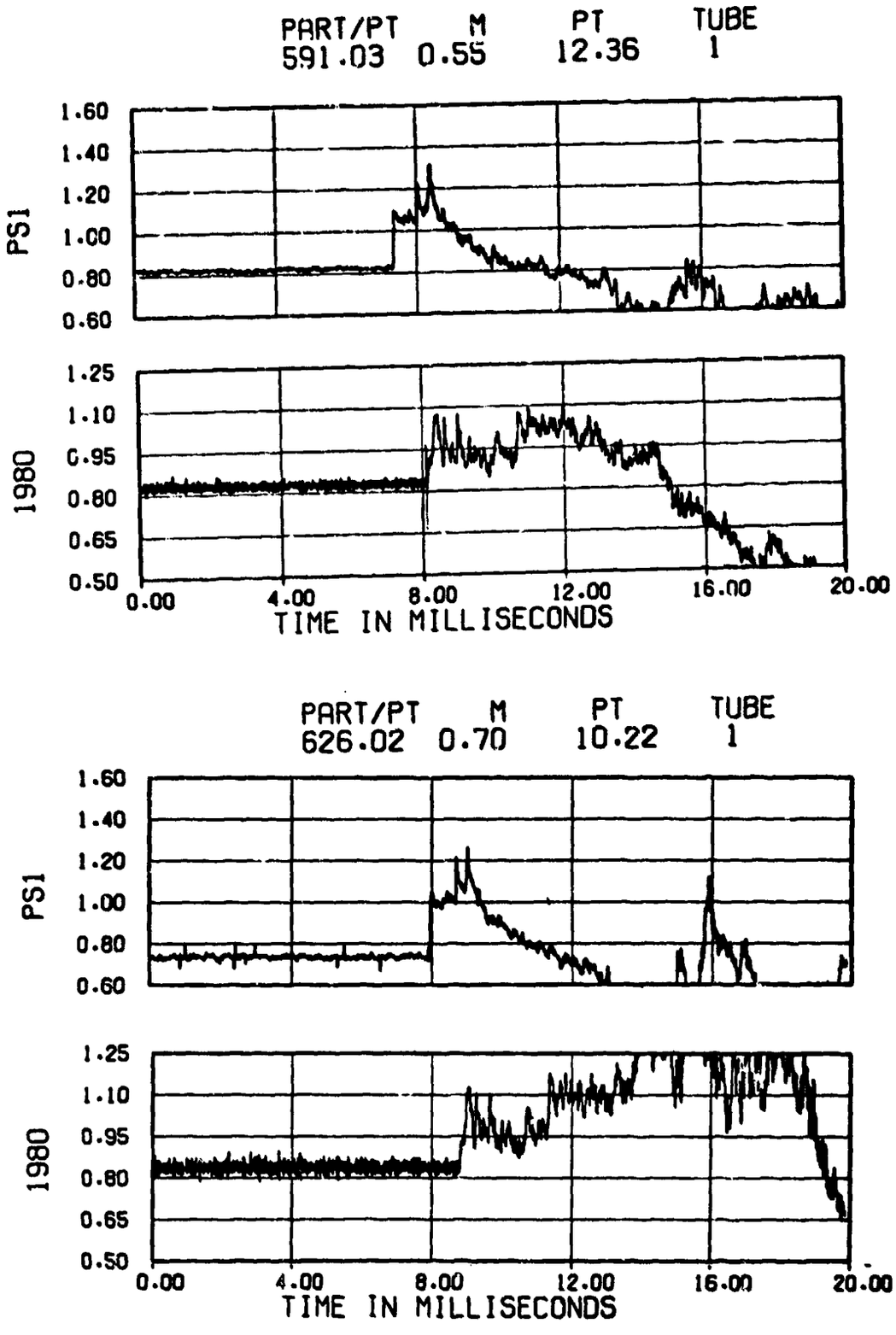

Figure 6 Comparison of Qualitative Characteristics of Claw Probe Static Pressure and Duct Static Pressure Histories For Shock Tube #1

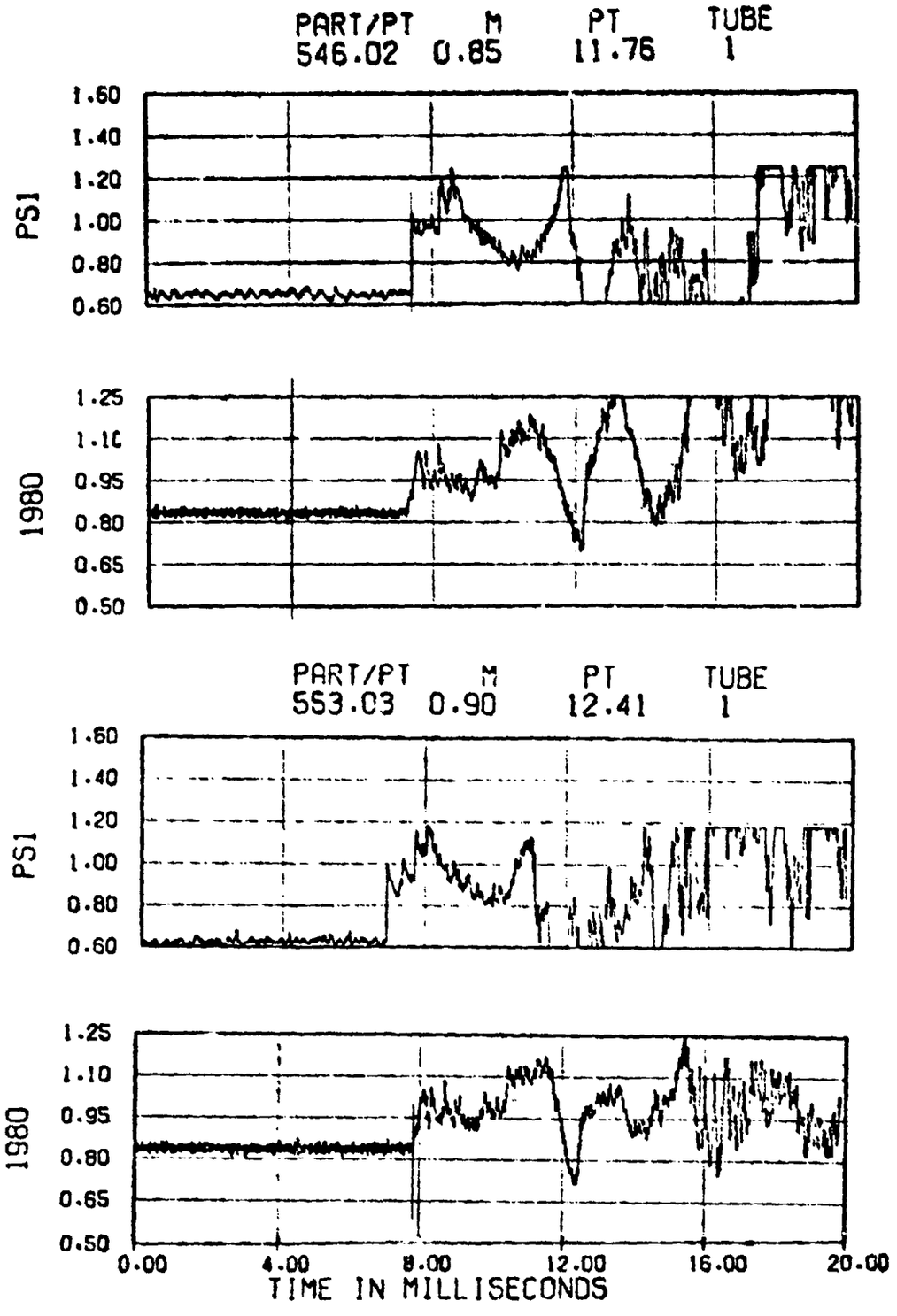

(Figure 6 Cont'd)

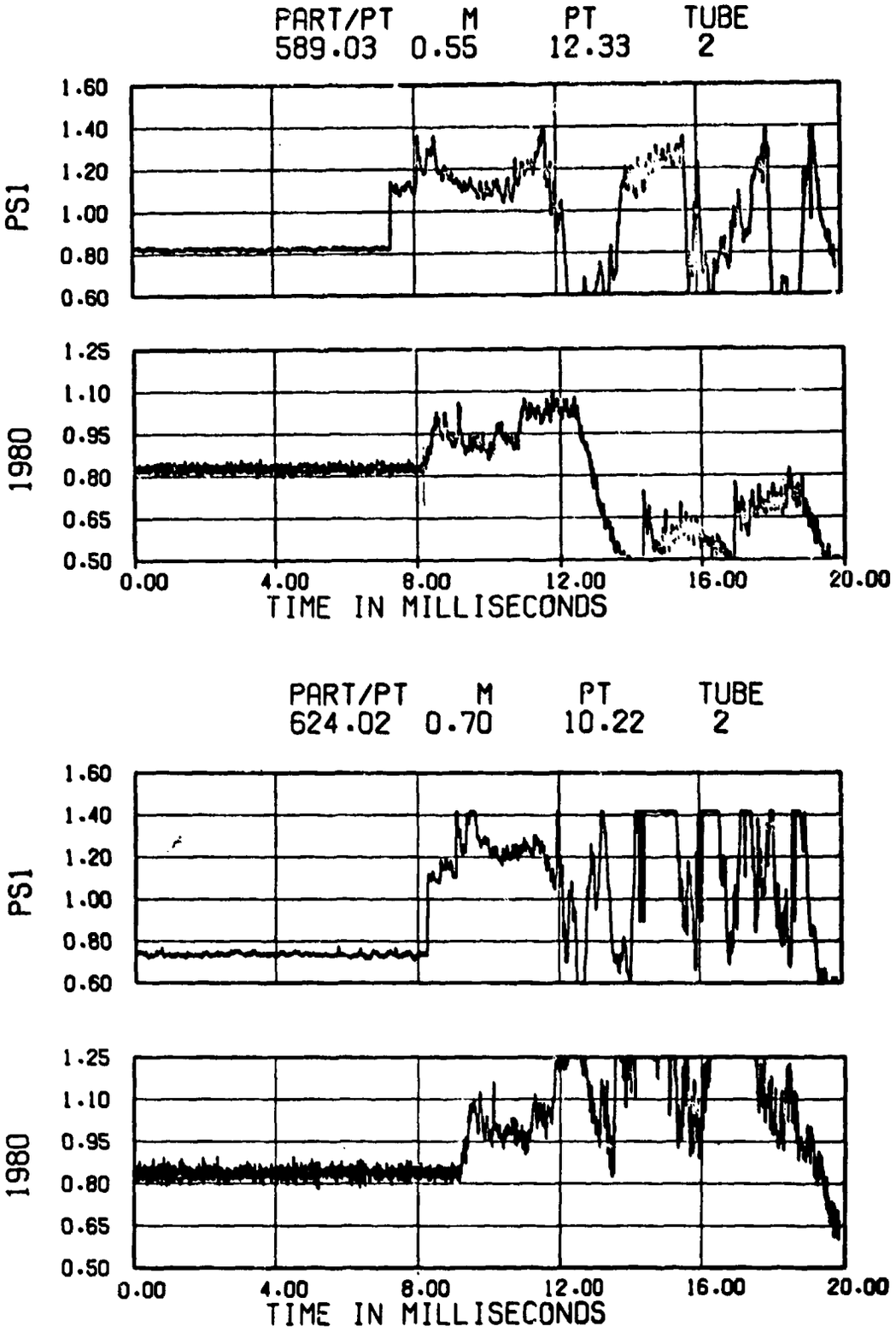

Figure 7 Comparison of Qualitative Characteristics of Claw Probe Static Pressure and Duct Static Pressure Histories For Shock Tube #2

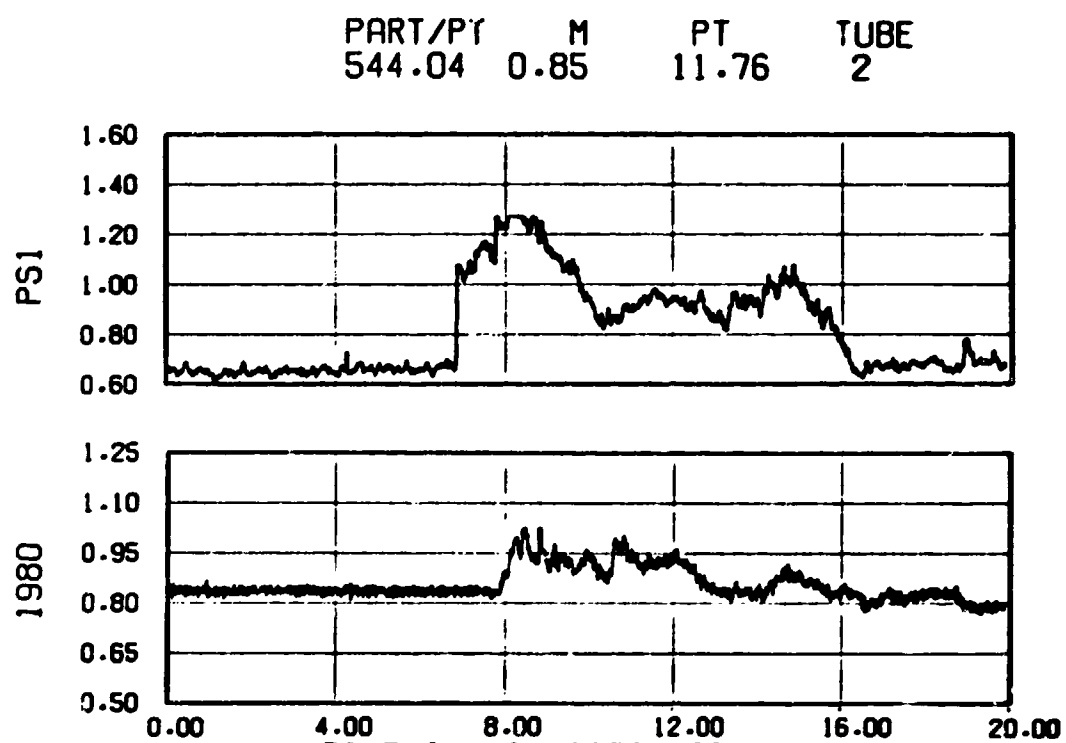

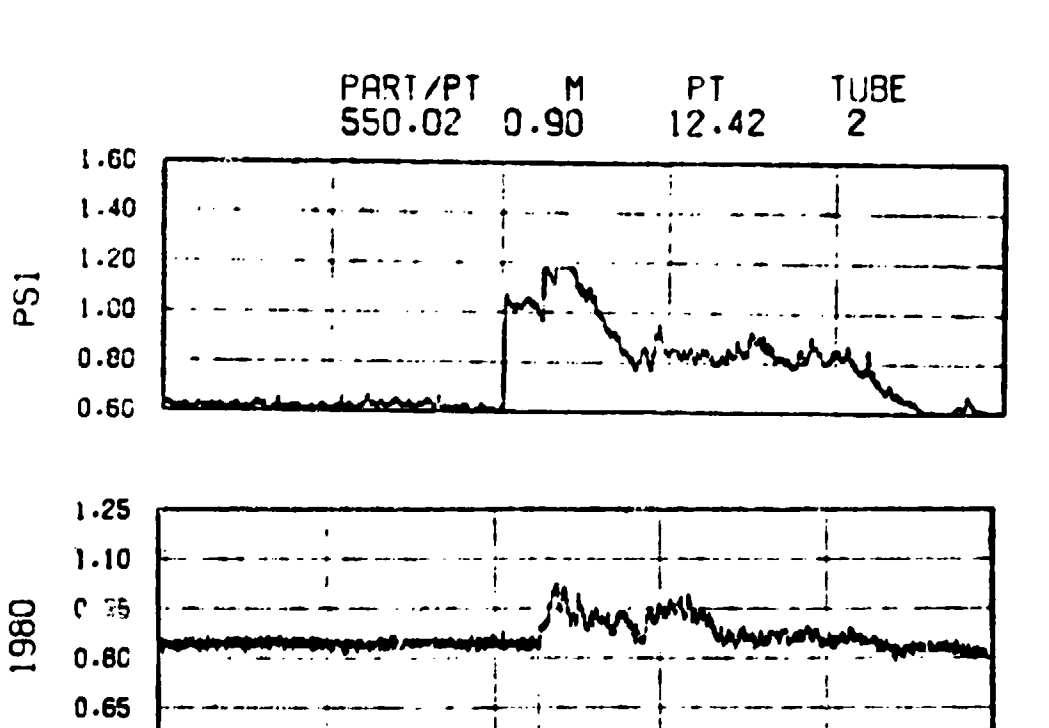

(Figure 7 Cont'd)

With the exception of the Mach number = 0.55 and 0.7 data for shock tube number 1, the time histories of the claw-probe and duct pressure transducers are similar suggesting that the shock-tube/free-stream flow characteristics are convected into the duct. The Mach number = 0.55, shock tube number 1 data are not alarming because what appears to be a second compression (occurring at about 10.3 milliseconds) reaches a level compatible with the maximum free-stream level and then falls off as the free-stream does. However, the Mach number = 0.7, shock-tube number 1 data illustrate a second compression near 11.5 milliseconds, which by itself is not a problem, but the ensuing compression is not consistent with the free-stream data. The reason for this duct static-pressure behavior at this isolated test condition is not understood. It is beyond the scope of the Calspan effort to determine if this apparent effect is real and what the associated explanation might be, but it is felt that such a study should be performed.

Typical time histories of the inlet-duct static pressure normalized by the tunnel free-stream total pressures for the inlet cowl surface are presented in Figure 8 where the numerical subscripts correspond to specific pressure transducers locations given on Figure 3. It was hoped that these data and those from the inlet ramp surface would have been useful for monitoring the behavoir of the shock-induced disturbance in the inlet duct. However, only PS 1902, PS 1935, PS 1905, PS 1970 and PS 1980 were considered by AEDC (Reference 21) to have valid calibrations. Unfortunately, PS1 was inadvertently plotted in place of 1935 and transducer 1970 didn't appear to be reliable. The remaining transducers PS 1950, PS 1903, PS 1904, PS 2902 and PS 1990 had erratic calibration response and thus the data from these transducers were considered to be questionable by AEDC personnel.

We analyzed the duct data in detail for 18 of the 43 tests but could not find a consistent behavior either in disturbance propagation speed or static pressure level. It was therefore concluded that the static-pressure measurements obtained in the inlet duct were of little use for determining shock-wave strength, pressure, or wave-propagation speed. However, as was discussed earlier in this section, these measurements were useful for demonstrating the compatibility between free-stream and inlet-duct flow characteristics.

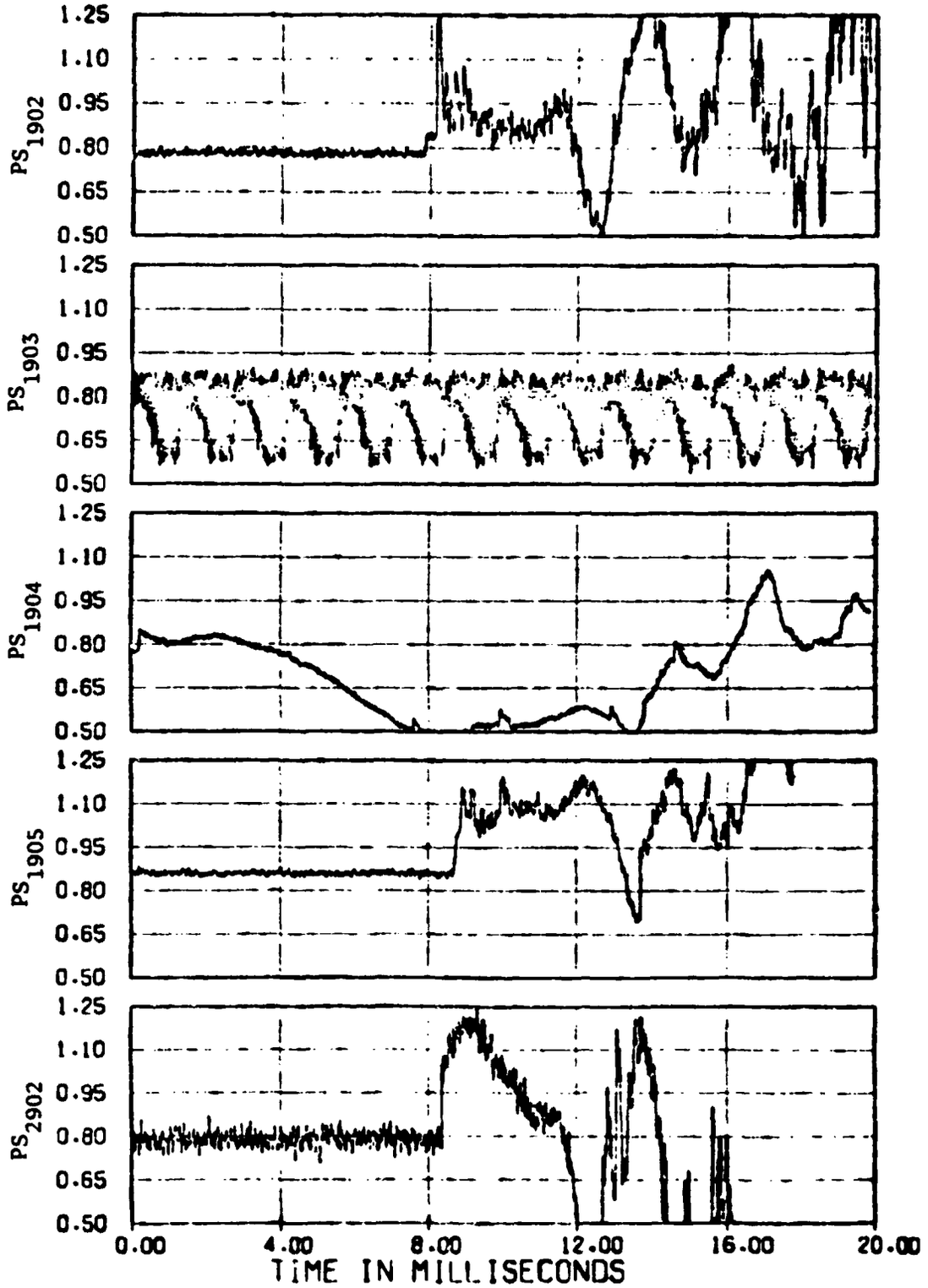

Figure 8 Inlet Cowl Surface Static Pressure Ratios Across the Incident Shock, M_o = 0.85 Part 546 Tube No. 1

5-1.3 Aerodynamic Interface Plane Total-Pressure Measurements

A complete set of outboard inlet AIP total pressures normalized by the tunnel free-stream total pressure is presented in Figures 9(a) through 9(h). The numbers in the pressure-ratio identification correspond to the dynamic-pressure probe locations at the A.I.P. Each figure represents a rake with the top trace being the probe nearest the hub and the bottom probe nearest the tip. The shock appears to be planar at the A.I.P., as may be seen by comparing the time of initial pressure rises and initial peaks on Figures 9(a) through 9(h).

As can be seen by comparing the results presented in Figure 5 and those presented in Figures 9(a) to 9(h), the outboard inlet pressure-ratio history at the AIP illustrate smaller pressure excursions and a greater effective test time than was determined from the windward claw probe PTC 1 or PTC 2. This would suggest that the duct has modified the character of the disturbance. Examination of Figures 9(a) through 9(h) indicates that all probes demonstrate an "N" wave characteristic during the first millisecond following the shock arrival. The maximum and minima of these traces occur at very nearly the same time on all AIP traces. The "N" wave is followed by a gradual decay lasting several milliseconds.

At the subsonic ramp setting the inlet has a throat located in the vicinity of Nacelle Stations (N.S.) 100-105. Hence, the incident shock is entering a converging-diverging duct. An attempt to calculate pressure ratios based upon the duct static pressures gave no meaningful results, because of the lack of definition of the incident-wave parameters and the questionable static-pressure data discussed earlier. A simple calculation based on continuity and the average "N" wave total pressure indicated that the inlet throat was probably choked for all of the test points except those for $M_o = 0.55$. The detailed behavior of the wave system in the inlet duct is an important consideration and should be studied further as noted earlier. Kaman AviDyne is in a position to apply their BID computer code to perform these detailed studies of duct wave-system behavior.

It is well known that a variety of wave systems could possibly be present in the duct depending upon the characteristics of the steady-state flow and the incident-wave strength. Several of these possibilities are discussed in detail in Reference 23. Similar "N" wave characteristics were obtained for tests using

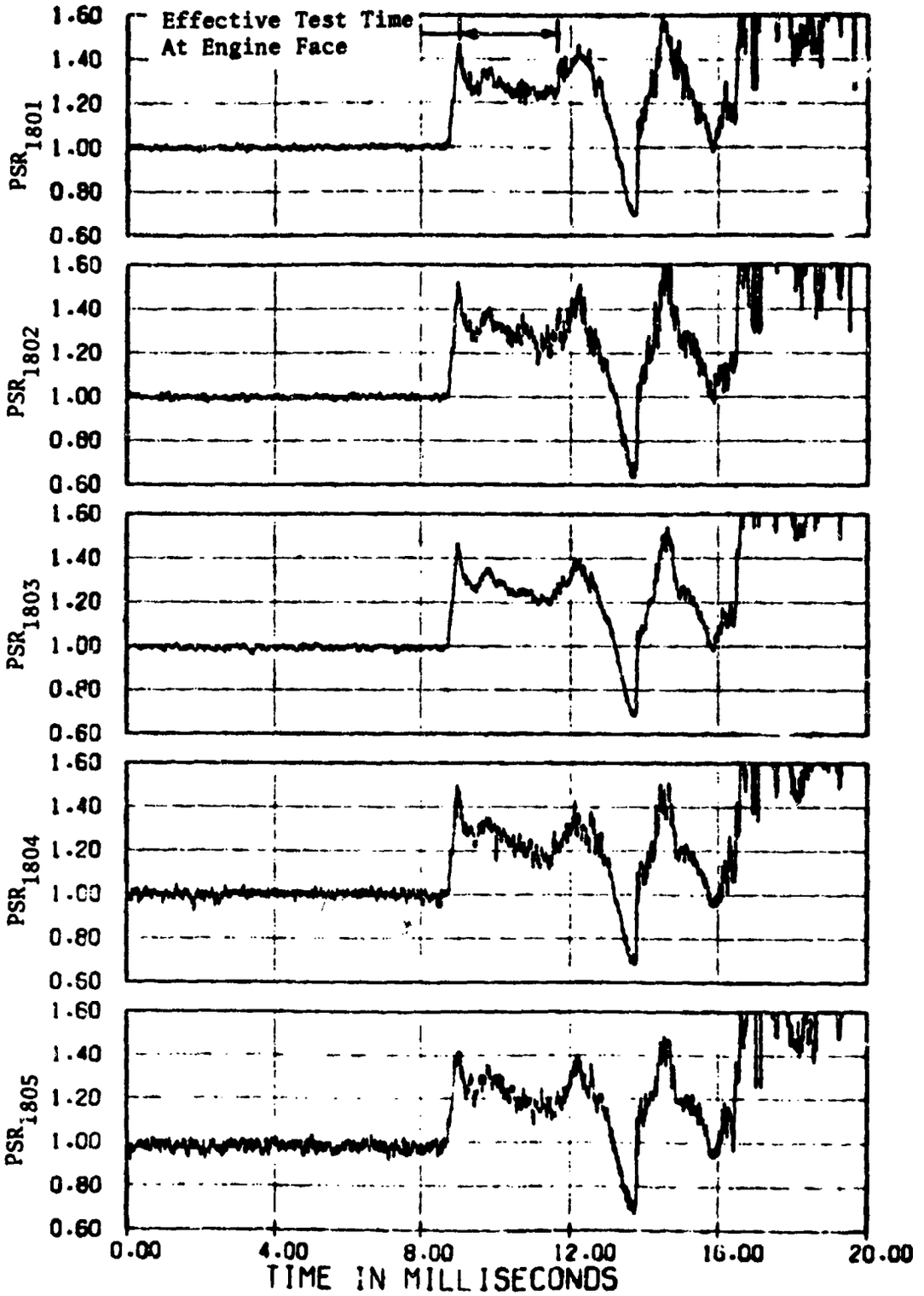

Figure 9(a) Outboard Inlet AIP Total Pressure Ratio Across the Incident Shock, M_o = 0.85 Part 546 Tube No. 1

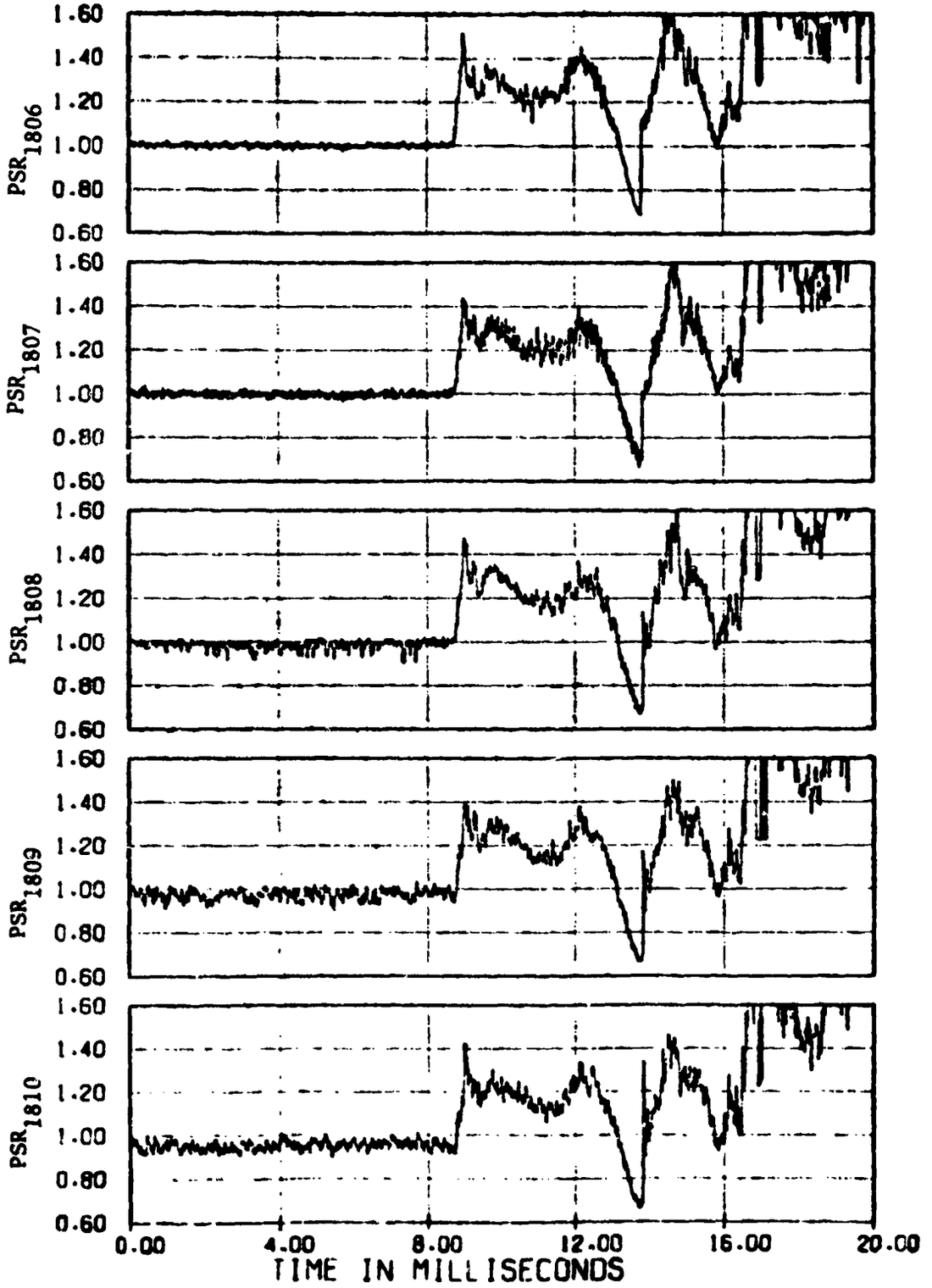

Figure 9(b) Outboard Inlet AIP Total Pressure Ratio Across the Incident Shock, M_o = 0.85 Part 546 Tube No. 1

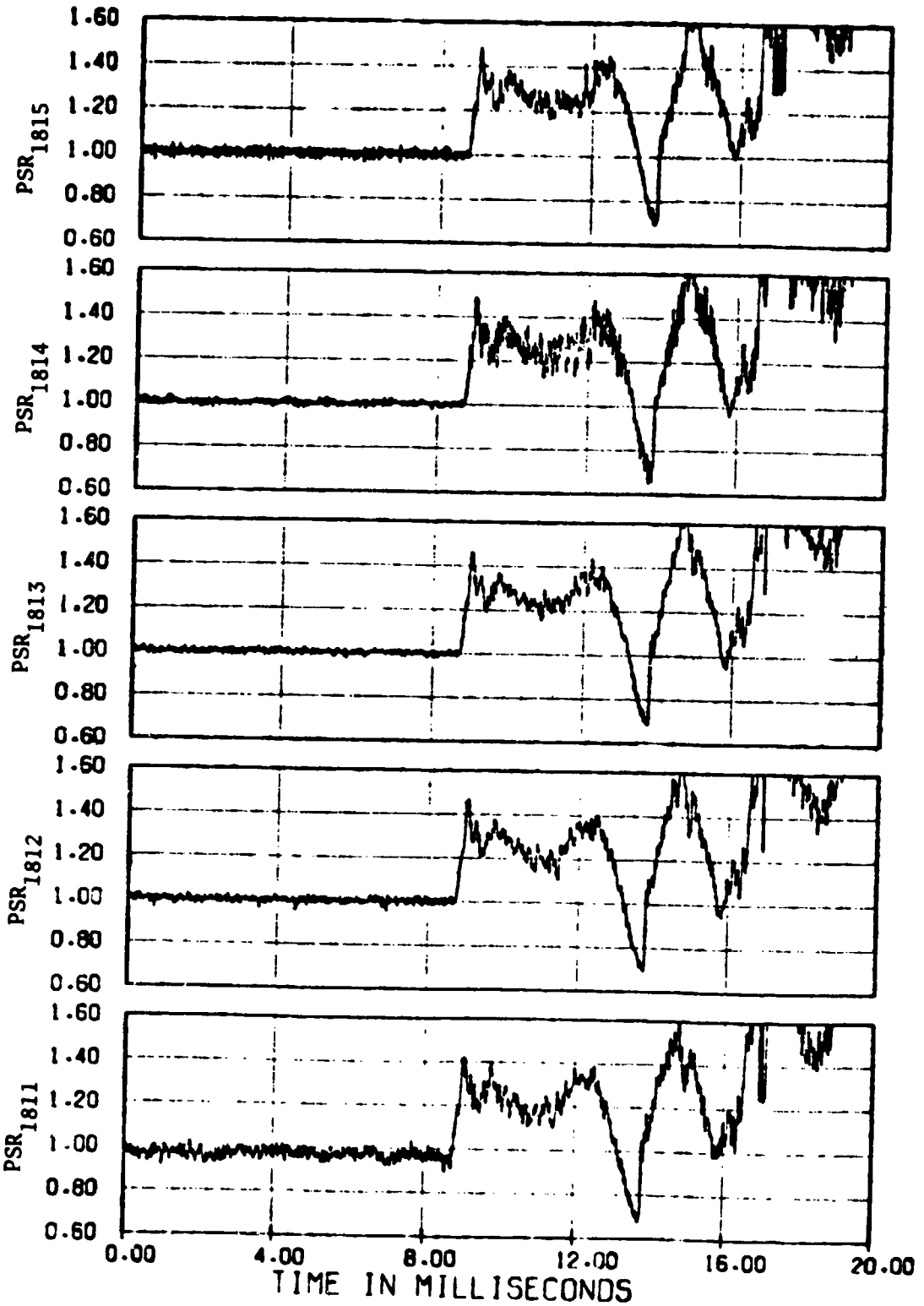

Figure 9(c) Outboard Inlet AIP Total Pressure Ratio Across the Incident Shock, M_o = 0.85 Part 546 Tube No. 1

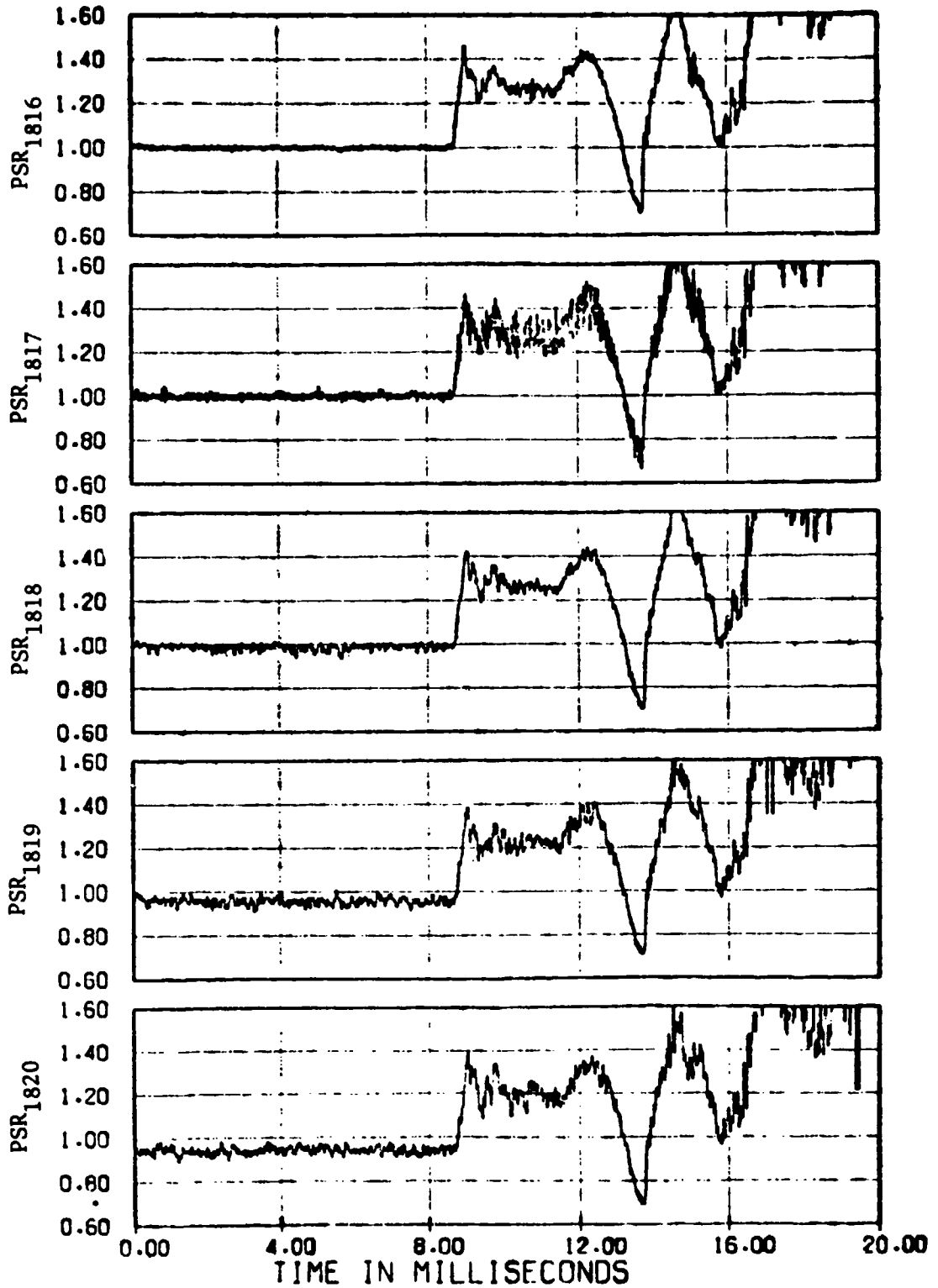

Figure 9(d) Outboard Inlet AIP Total Pressure Ratio Across the Incident Shock, M_o = 0.95 Part 546 Tube No. 1

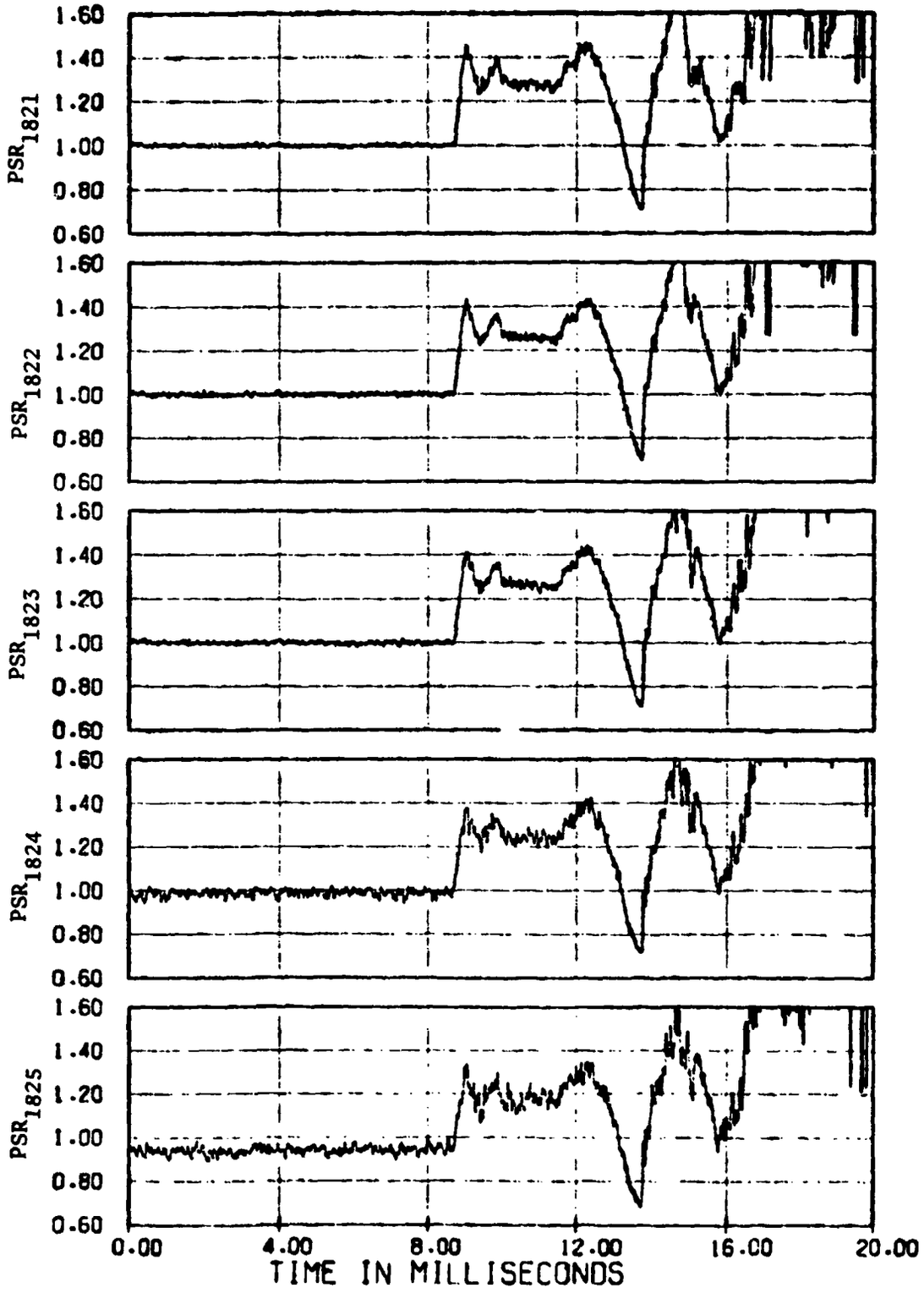

Figure 9(e) Outboard Inlet AIP Total Pressure Ratio Across the Incident Shock, M_o = 0.85 Part 546 Tube No. 1

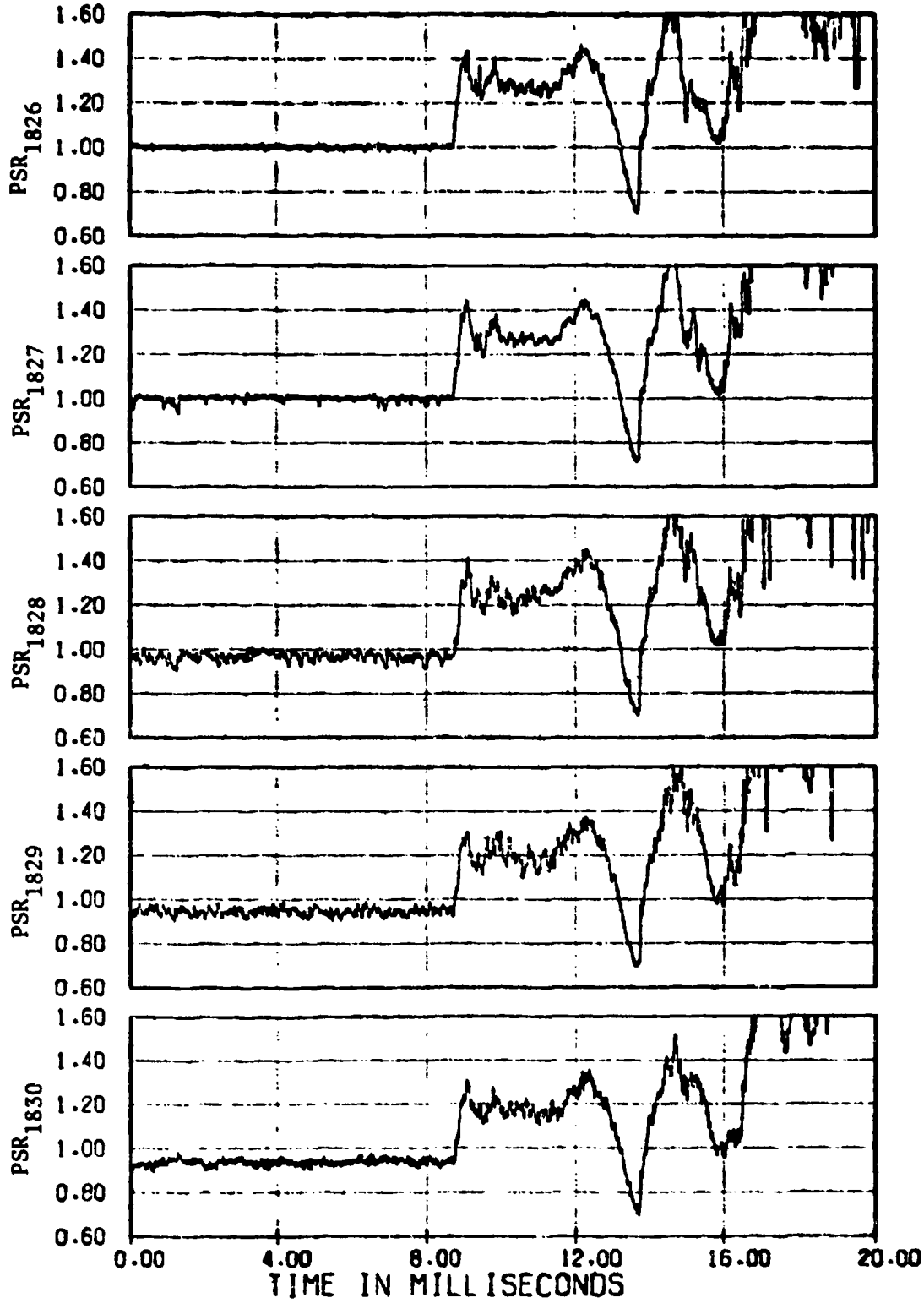

Figure 9(f) Outboard Inlet AIP Total Pressure Ratio Across the Incident Shock, M_o = 0.85 Part 546 Tube No. 1

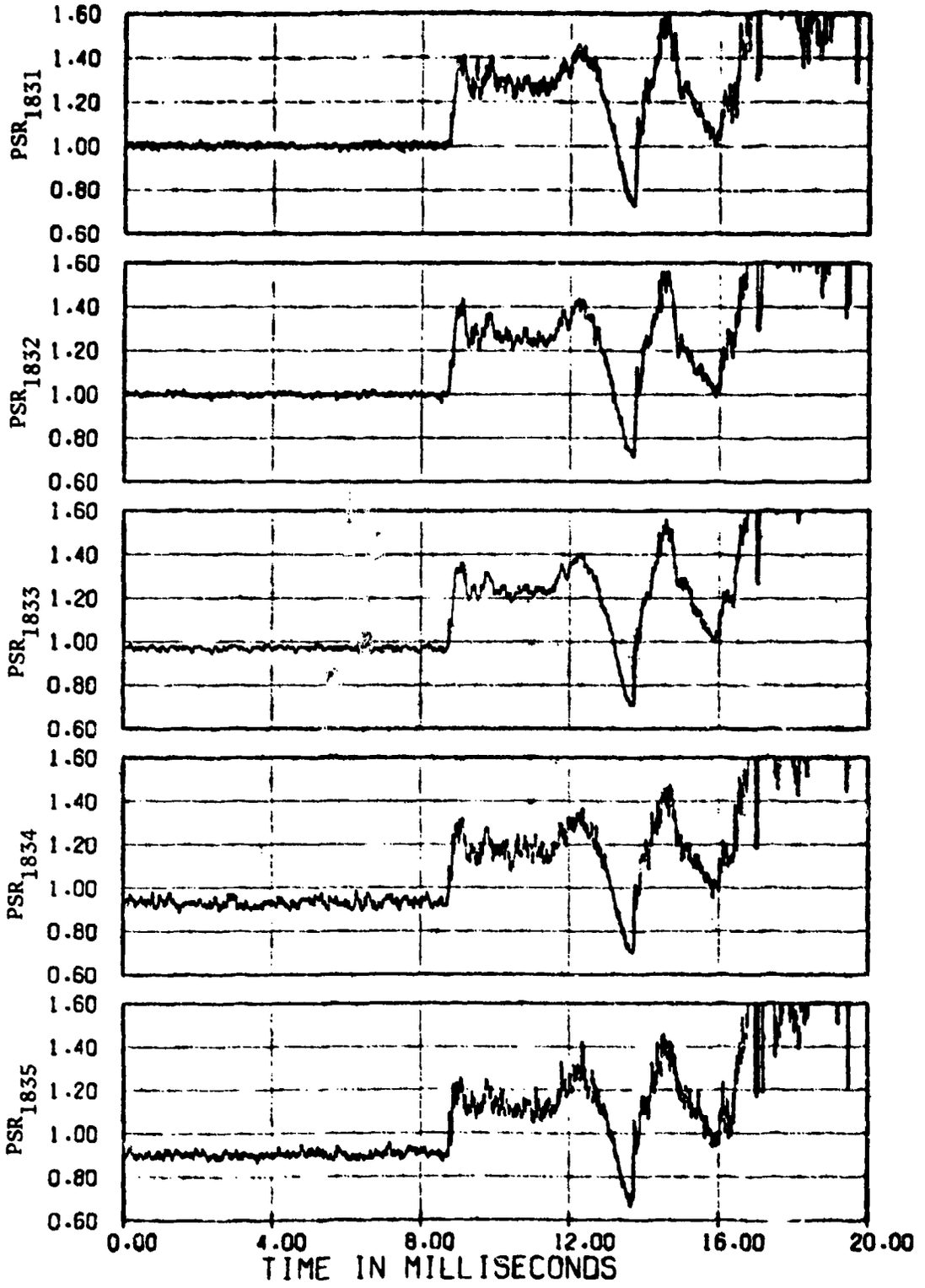

Figure 9(g) Outboard Inlet AIP Total Pressure Ratio Across the Incident Shock, M_o = 0.85 Part 546 Tube No. 1

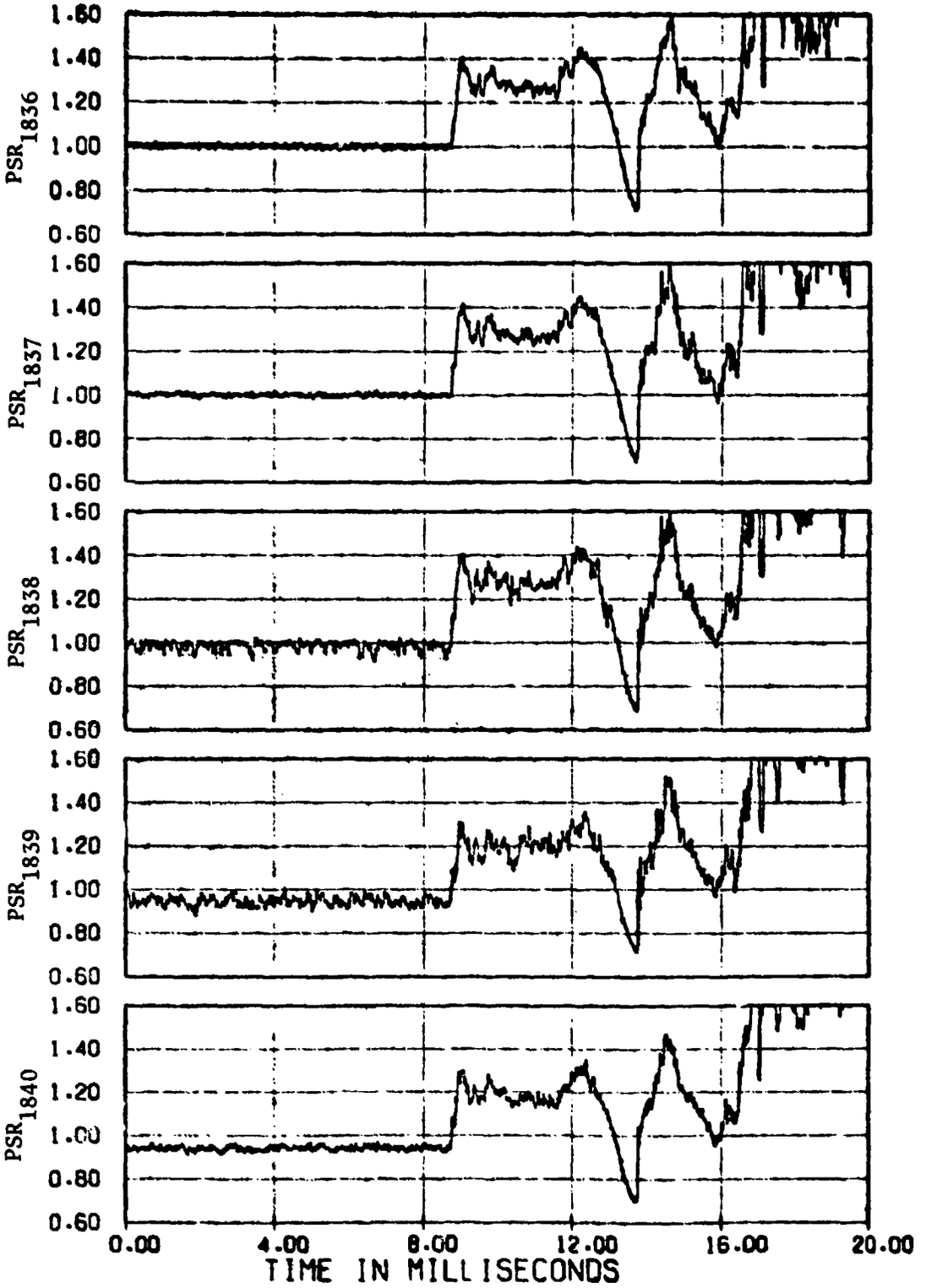

Figure 9(h) Outboard Inlet AIP Total Pressure Ratio Across the Incident Shock, M_o = 0.85 Part 54f Tube No. 1

shock tubes #2 and #3. The "N" wave characteristic was also noted in Part 501 where there was no wind-tunnel flow.

The inboard (leeward) inlet demonstrated AIP PSR traces very similar to those of the claw PTC3 (see Figure 3) as shown in Figures 10(a) and 10(b). This behavior is typical of all leeward AIP traces for all three shock-tube firings. The maximum PSR is considerably less than that of the windward side AIP PSR's because of attenuation of the incident wave by the inlet structure. Although only two rakes are shown to illustrate the leeward AIP response, the remaining probes had a similar response, i.e. a planar wave at the AIP.

The averaged AIP pressure ratios (R1) for both inlets are shown in Figure 11. For the purpose of distortion analyses only the outboard AIP data are of major significance, because of the greater pressure ratios. The R1 traces used in conjunction with the claw probe data were used to select the time intervals believed to be valid of distortion analysis. On this basis, we feel that the initial 1.2 milliseconds after shock arrival is the appropriate test time. However, the character of the duct flow has been modified so that one could reasonably use the time interval labelled "effective test time" on Figure 11 for the purposes of distortion analysis. One would obviously like to have a greater period of time but for the purposes of these experiments the time realized was felt to be acceptable. The time interval selected is larger than that indicated for the claw probe PCT1 in Figure 5. It should be noted that extension of the valid test time interval is somewhat arbitrary. Data beyond the test interval contains highly turbulent flow probably resulting from the shock-tube internal-wave action and should not be used for distortion analysis.

5-1.4 Distortion Data

The radial distortion (IDR), circumferential distortion (IDC), and stall margin (IDL) are presented in Figures 12(a) and 12(b) for Part 546. Presentation of the IDR's and IDL's for the individual rakes and rings is beyond the scope of this report. However, the trends in all tests were similar, in that both distortion indices are tip concentrated. This is to be expected since the pressure deficit is primarily a result of shock wave - boundary layer interaction. The

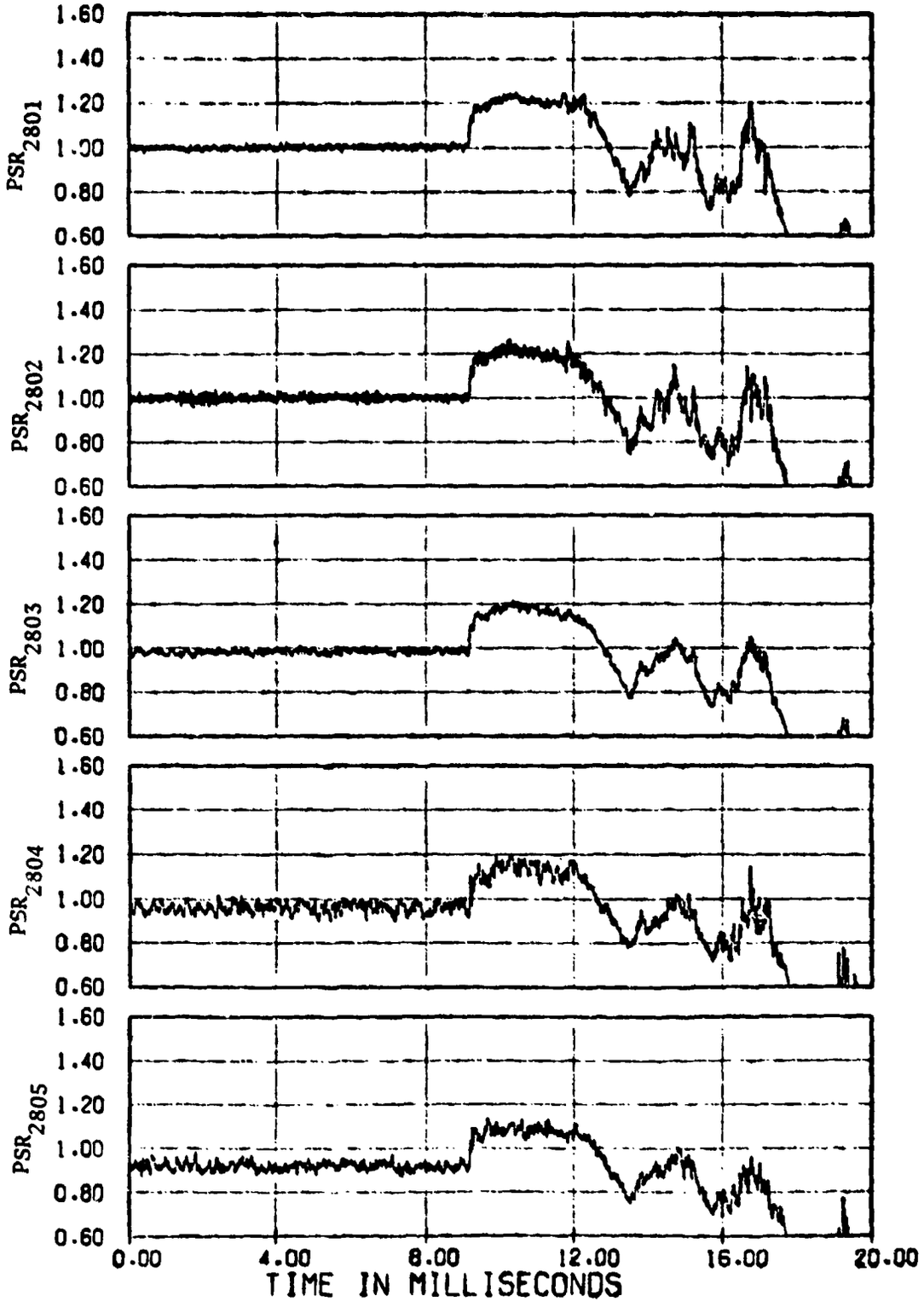

Figure 10(a) Inboard Inlet AIP Total Pressure Ratio Across the Incident Shock, M_o = 0.85 Part 546 Tube No. 1

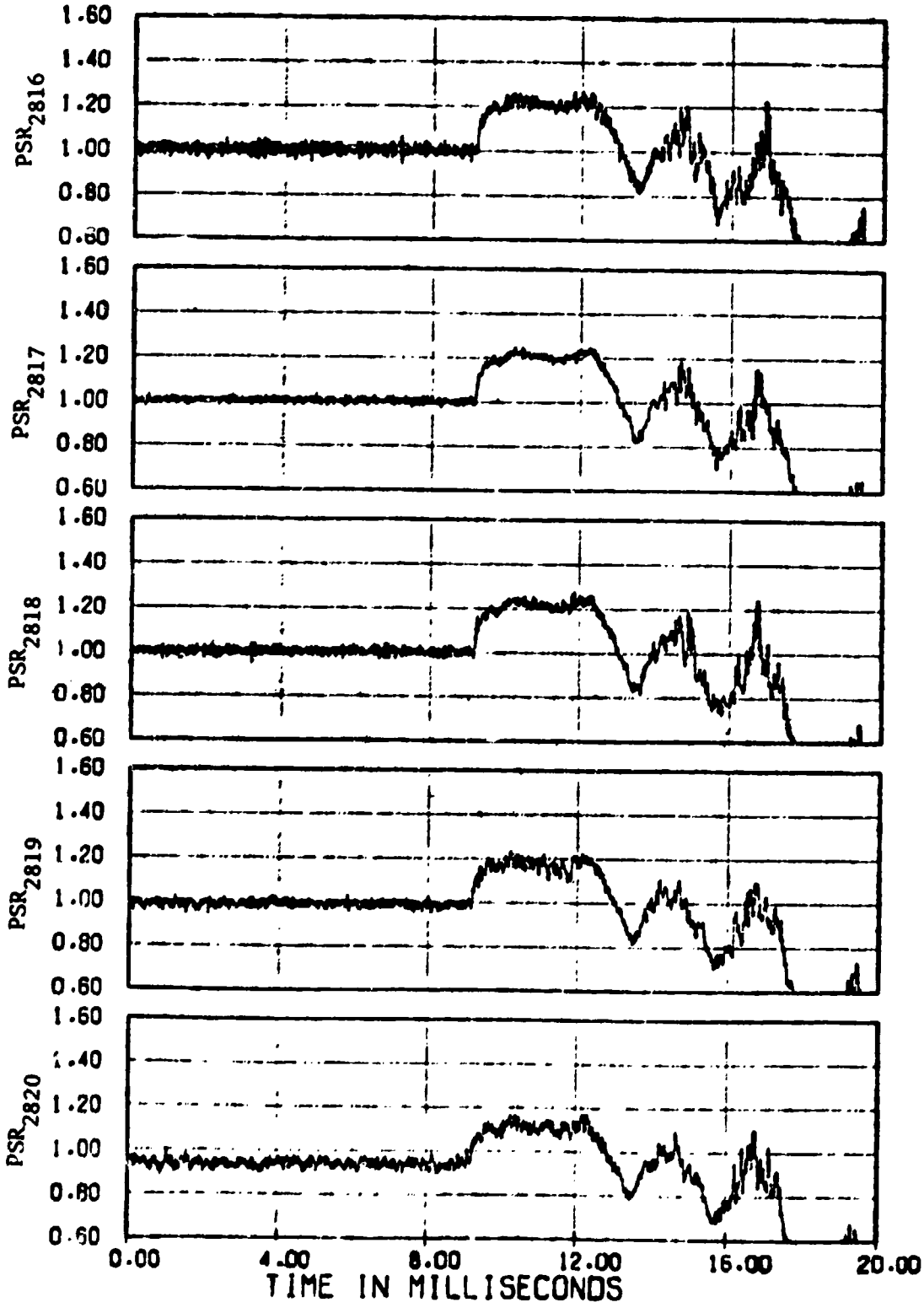

Figure 10(b) Inboard Inlet AIP Total Pressure Ratio Across the Incident Shock, M_o = 0.85 Part 546 Tube No. 1

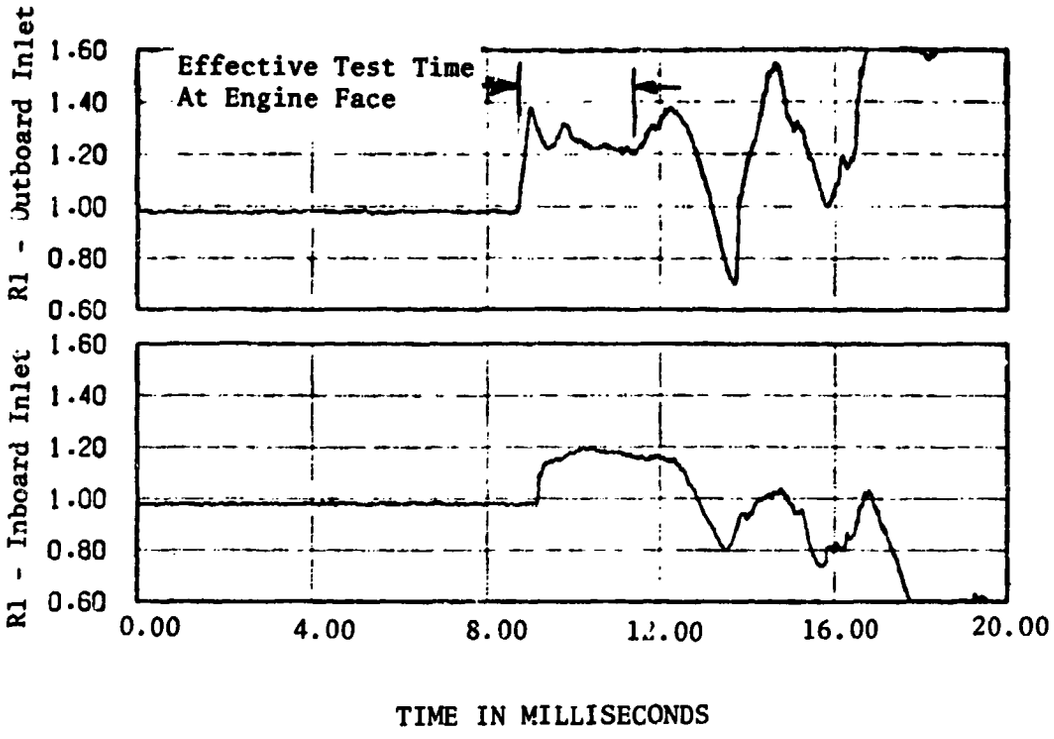

Figure 11 Average AIP Total Pressure Recovery, M_o = 0.85 Part 546 Tube No. 1

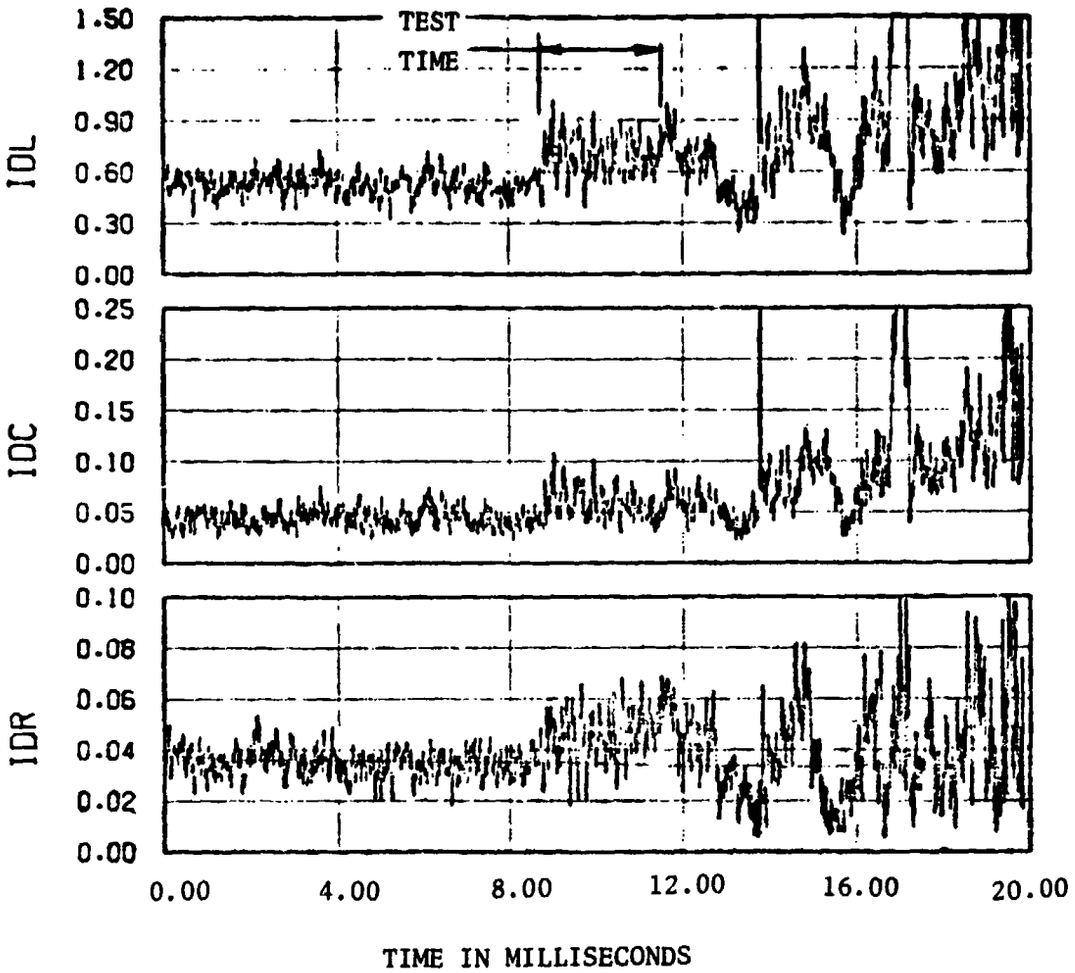

IDL = 1 MEANS THAT INLET STALL MARGIN HAS BEEN EXHAUSTED AND STALL IS POSSIBLE

Figure 12(a) Outboard Inlet Distortion Indices, M_o = 0.85 Part 546 Tube No. 1

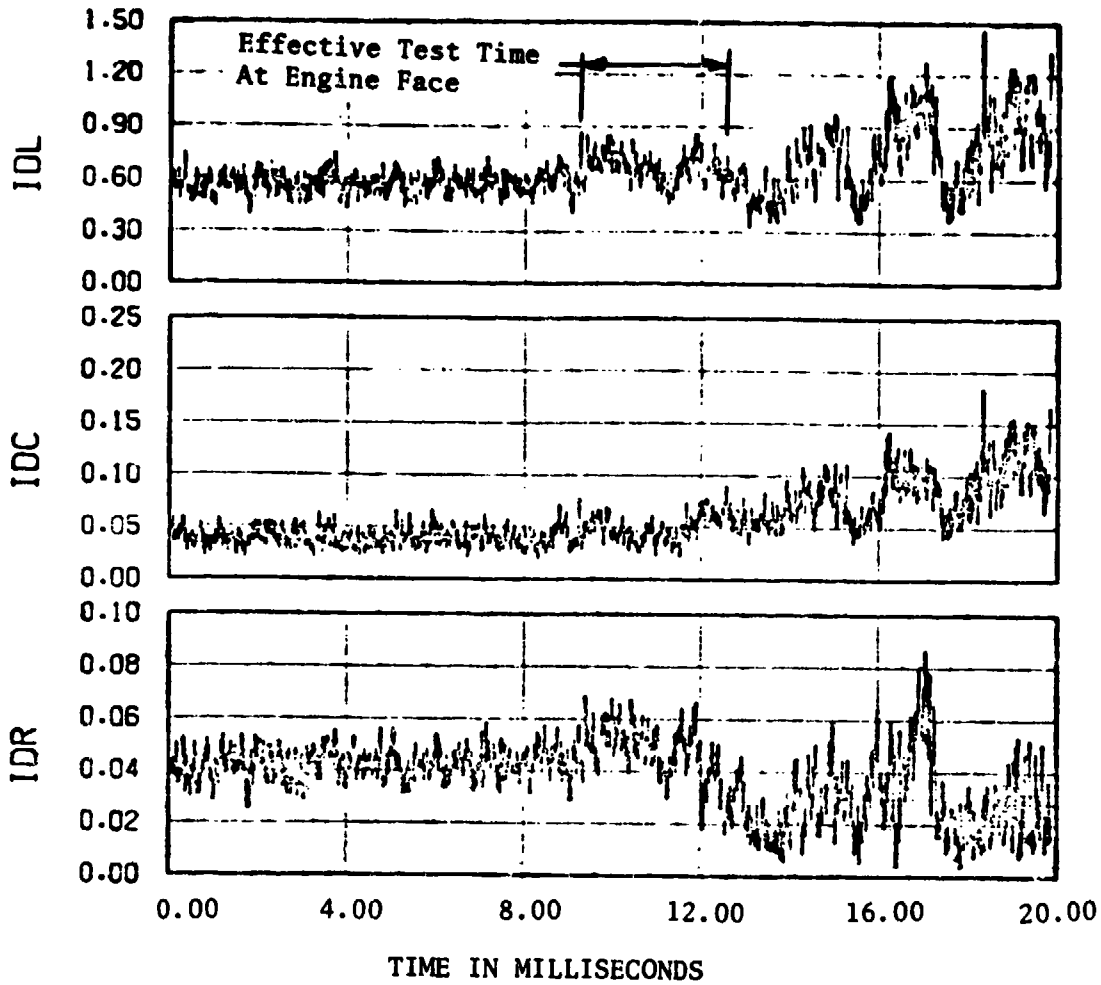

Figure 12(b) Inboard Inlet Distortion Indices, M_o = 0.85 Part 546 Tube No. 1

method of determining IDR, IDC, and IDL is given in References 7 and 8. The test-time interval indicated on Figure 12(a) is the same as that of Figure 10. Increased dynamic activity of both IDR and IDL upon the arrival of the transmitted shock is evident. The radial mode (IDR) appears to dominate. A peak IDL of 1.05 is attained early in the test period. In the cited case, this corresponds to the first peak of the transmitted wave. Examination of the other test points indicates that the occurrence of the maximum IDL is random, i.e. it may occur anywhere in the test period depending upon the relative magnitudes of IDR and IDC. Higher peaks in the distortion indices following the test interval are a result of the aforementioned highly turbulent flow and have no bearing upon the test results.

The inboard inlet-distortion indices for Part 546 are presented in Figure 12(b). It is apparent from the peak IDL values that blast-induced distortion is not a problem in this inlet. A similar behavior was exhibited for all leeward inlets in the test program.

5-2 COMPARISON WITH PREVIOUS DISTORTION DATA

Extensive distortion test data are available for the B-1 inlet system. Wind-tunnel tests have been conducted with models of 0.1, 0.2 and full scale. The AIP instrumentation locations were identical for models of all scales. The 0.1-scale model was previously tested in the Rockwell Transonic Wind Tunnel (TWT), while the 0.2 and full-scale tests were conducted by Rockwell in the AEDC 16T tunnel. In Figures 13(a) and 13(b) the distortion parameters obtained in the Kaman/AEDC tests at times prior to the arrival of the transmitted shock are compared with data from previous B-1 inlet model tests. The scale effect data are taken from Reference 12. The corrected airflow ratios are referred to a nominal corrected airflow of 357 lb/sec. The pre-shock dynamic distortion indices obtained in the present test program are a little larger than those obtained during previous tests. This difference can be explained on the basis of the data filtering process used during the previous test programs and will be discussed in greater detail in the following subsections. The correlation between the dynamic-distortion indices of the Kaman/AEDC experiments is considered to be good and the pre-shock dynamic data obtained during the present test program are consistent with those previously obtained by Rockwell in other test programs using the same and other models.

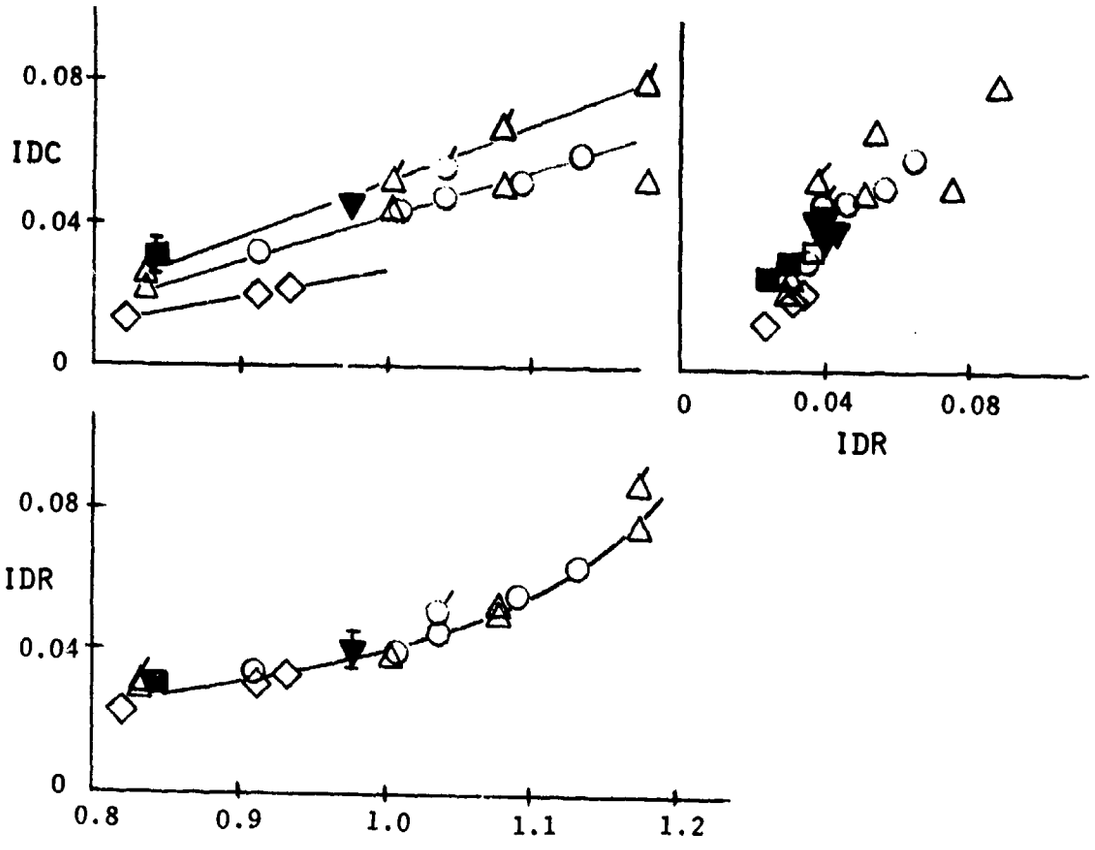

Symbol	Test	Part	Model Scale
○	TWT	304	0.1 Rockwell
△	TF	147	0.2 Rockwell/AEDC
◇	TF	2225	1.0 Engine
■	TF	606,607	0.1 Kaman/AEDC
▼	TF	544-546 619-620	0.1 Kaman/AEDC

$M_o = 0.85$

Flags Denote Peak IDL

Figure 13(a) Model Scale Effect on Distortion

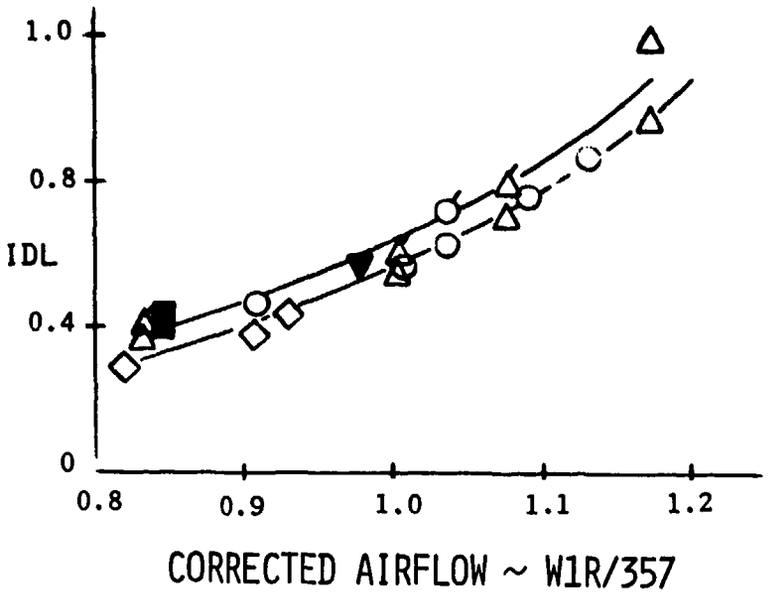

Symbol	Test	Part	Model Scale
○	TWT	304	0.1 Rockwell
△	TF	147	0.2 Rockwell/AEDC
◇	TF	2225	1.0 Engine
■	TF	606,607	0.1 Kaman/AEDC
▼	TF	544-546 619-620	0.1 Kaman/AEDC

$M_0 = 0.85$

Figure 13(b) Model Scale Effect on Stall Margin Index

The influence of Reynolds number upon the distortion indices is illustrated in Figure 14. Here again, data from the present test are superimposed on data from Reference 12. The Reynolds number is based on free-stream conditions and the length from the cowl lip to the engine face. The data of Reference 12 were based on a nominal W1R = 357 lb/sec, while those from the present test have a W1R = 350. Distortion indices decrease with decreasing values of W1R, hence the present test data are considered to be in good agreement with the data from Reference 12. The slightly higher value of the peak dynamic IDL will be discussed in the next subsection.

5-3 DISTORTION TEST RESULTS

5-3.1 Distortion Methodology and Inlet/Engine Compatibility

As mentioned earlier, engine stall or surge may be caused by pressure or temperature defects at the engine face. In the present test program only the pressure defects are considered because they are the more important of the two parameters. Temperature-defect distortion has not received the attention that pressure distortion has and thus a comparable methodology does not exist at the present time. In the following discussion, distortion will always refer to pressure distortion. By convention the stall margin is defined as the difference between the engine operating-line pressure ratio and the surge-line pressure ratio at constant corrected weight flow as shown in Figure 1. However, as mentioned in Section 3, for the short times associated with blast waves, one should move along a line of constant rpm. The stall margin is usually apportioned between the engine and the inlet by agreement between the airframe and engine manufacturers. Therefore, an IDL = 1.0 indicates that the inlet stall margin has been exhausted and a stall is possible. Whether the engine stalls or not depends upon how much of the engine-chargeable stall margin remains.

Distorted flow entering the engine has the effect of lowering the surge line and thereby reducing the stall-margin. The distortion indices referred to herein were derived by General Electric and are known as Method D. For details

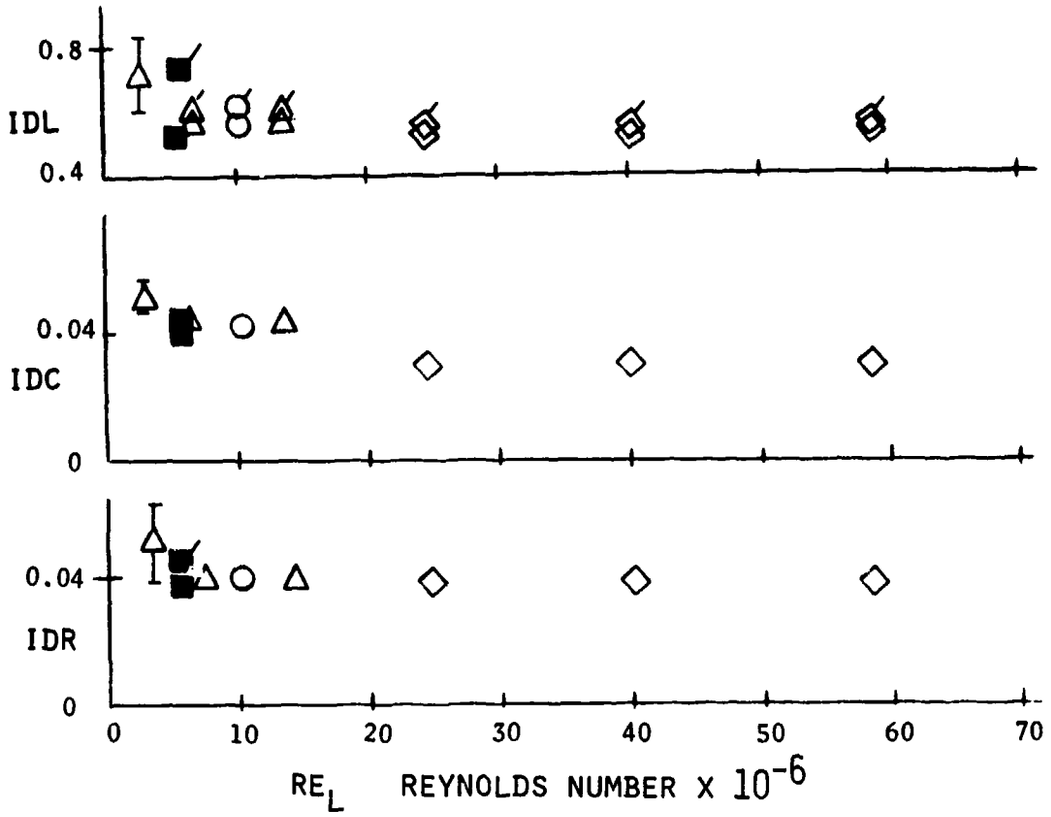

Symbol	Model Scale
○	0.1 Rockwell
△	0.2 Rockwell
◇	1.0 Engine Rockwell
■	0.1 Kaman/AEDC

Flagged Symbols are Dynamic Peak Values

$M_0 = 0.85$

Figure 14 Summary of Reynolds Number and Scale Effects

of the development of this method see References 6 and 7. Method D is empirically derived, using pressure defect parameters to describe distortion patterns. This distortion is then related to the surge loss by defining coefficients or sensitivities. Once the sensitivities are determined, they can be used to predict stall-margin pressure loss and assess engine stability for a given inlet distortion pattern. Method D has been under development since 1970 and has given a reasonably good prediction of engine stall for both the F101-GE-100 and J85 engines (Reference 7).

Both steady-state and dynamic-distortion effects are calculated using Method D. To calculate dynamic distortion an additional parameter, the data frequency content, is required. This parameter relates the peaks in the calculated stall-margin to the experimentally measured available stall-margin. Use of frequency content introduces the concept of critical time of critical frequency. This is usually defined at the maximum pressure-pulse frequency or time to which the engine will respond. For the F101-GE-100 engine, all existing B-1 dynamic distortion index computations (Reference 12) were filtered as near as possible to the full-scale critical frequency of 62.5 Hz (0.016 sec) or one fan-blade revolution. The critical frequency is defined in the following manner: the time period for one fan-blade revolution is $\Delta t = 60/7500 = 0.008$ seconds, this value is then the period for a one-half wave form giving a full wave the period of 0.016 seconds. This point is also defined from the filter characteristics as the ratio of frequency to the critical frequency where the amplitude ratio is down -3 dB. Once the critical frequency is known, the analog pressure data is filtered to this frequency with a low-pass analog or digital filter and stall margins may be determined. Use of unfiltered pressure data may lead to spurious stall indications, because the engine does not respond to the higher frequencies. On this basis, it is possible to draw the very important distinction between inlet distortion and inlet/engine compatibility. The present Kaman/AEDC data have been analyzed as inlet distortion data but the previous Rockwell data were analyzed using detailed filtering procedures to obtain inlet/engine compatibility results.

In the Rockwell wind-tunnel and flight tests the FM-tape data were filtered with a Bessel linear-analog low-pass filter and digitized at a rate of approximately four times the filter cut-off frequency. A moving average was then applied

to the digitized data. The number of the samples used in the moving average is known as the window size. Generally, the average is advanced one data increment for each average. The moving average acts as a digital filter in a manner closely analogous to a 5-pole linear phase analog filter (Reference 7). The effect of digital filtering upon IDL is shown in Figure 15 taken from Reference 23. The data are for the 0.1 scale B-1 inlet at M_o = 2.2 and a digitizing rate of 8000 samples per second. Examination of the data indicate a small time shift and reduction in the peak IDL's as the size of the moving windows is increased, i.e. the top trace is data at the digitizing rate and the bottom trace is the dynamic average computed at 2 fan-blade revolutions or the maximum window size of 14. The single fan-blade revolution data corresponds to a window size of 7. This value includes model scale effect, where the frequency scales as the length and is related to the Strouhal number (fL/V). Scaling effects are discussed in some detail in Reference 13. The reduction of peak IDL with window size is shown in Figure 16. The reduction in IDL with increasing window size is seen to be exponential. The data points in Figure 16 correspond to the traces in Figure 15.

Data showing the effects of filtering frequency for the 0.1 scale B-1 inlet model at M_o = 0.85 are given in Figure 17. These data are from Reference 13 and were analyzed on a slightly different basis than those of the preceding figures. Here 57.5 Hz corresponds to the 1 fan-blade revolution. It should also be noted that the mean and steady-state values are quite close. It is evident that the inlet distortion data must be filtered to eliminate data to which the engine will not respond and which could give spurious stall indications.

5-3.2 AEDC Wind-Tunnel Test Results for ΔP of 2.0 and 2.5 psi

The wind-tunnel test data for the blast-wave overpressures (ΔP) of 2.0 and 2.5 psi will be discussed herein. Data obtained at overpressures less than 2.0 were not considered to be significant in terms of inlet distortion because of the low measured values of IDL. This is a hindsight observation of the results and is not intended to imply that the lower overpressure experiments should have been deleted from the test matrix.

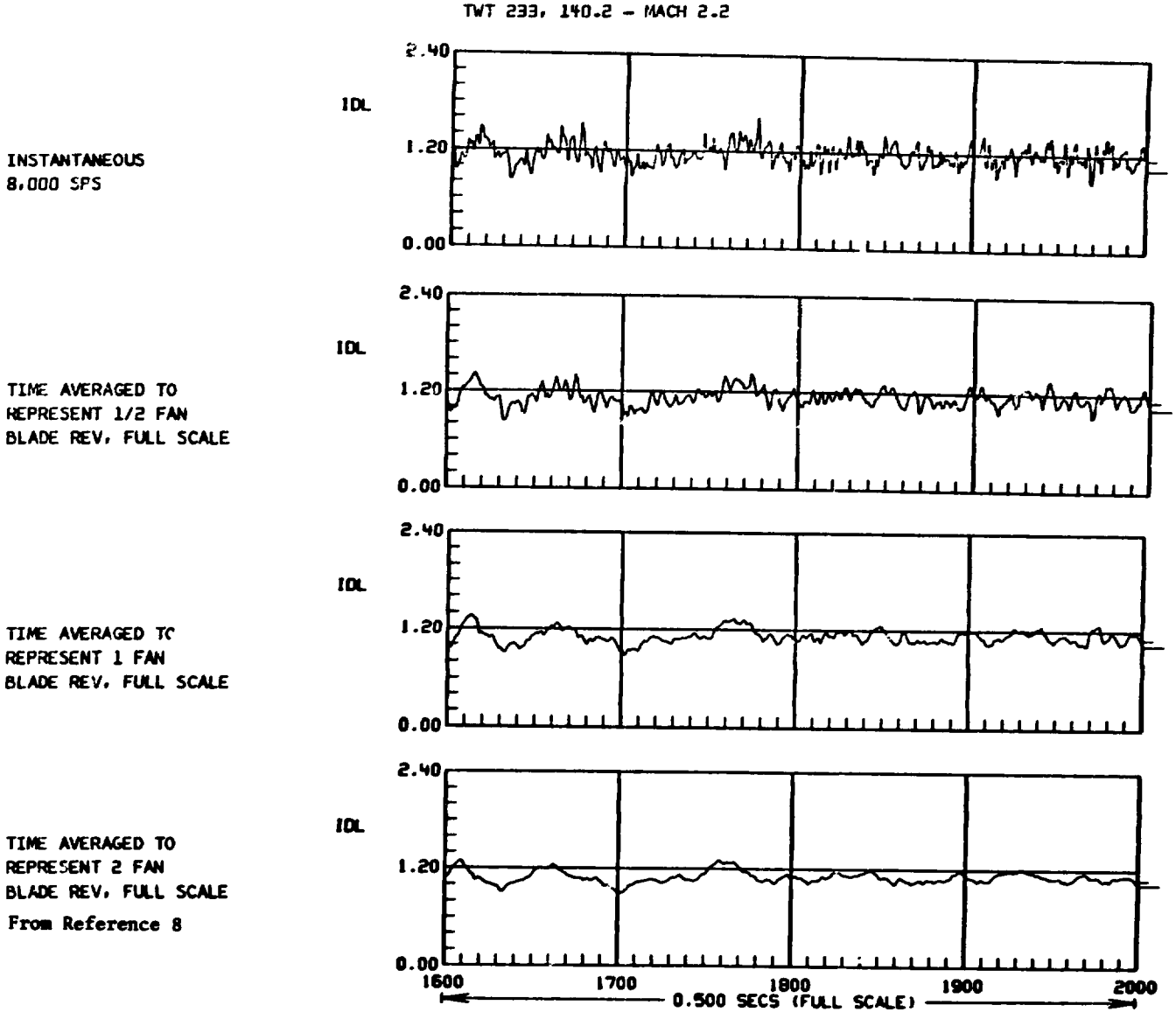

Figure 15 Digital Stall Margin Ratio Versus Time, Filtered to Various Frequency Levels

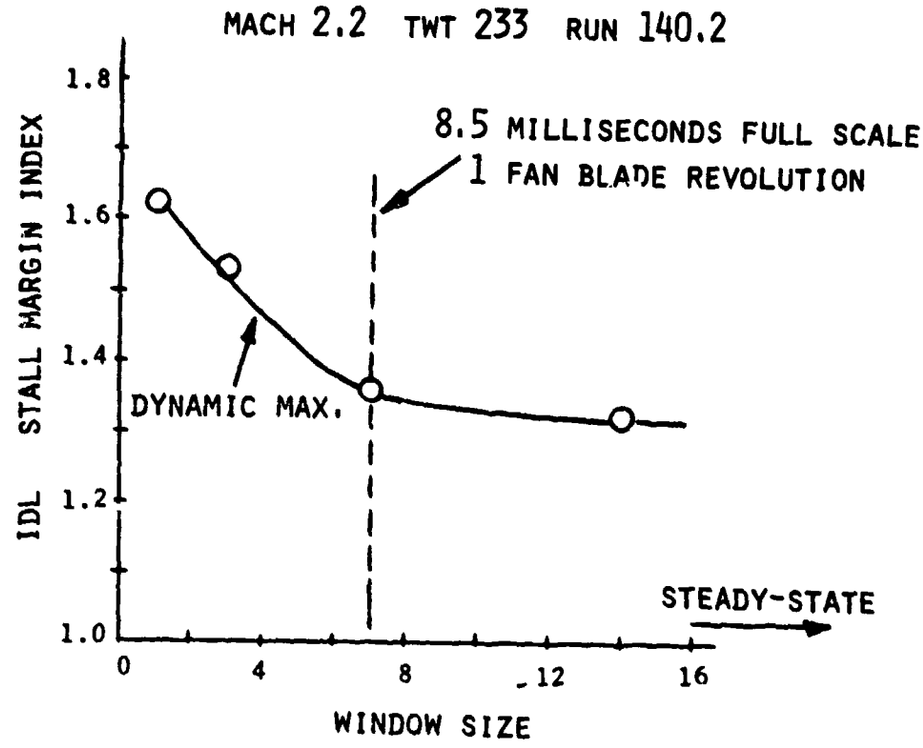

Figure 16 Influence of Time Averaging on Stall Margin Index

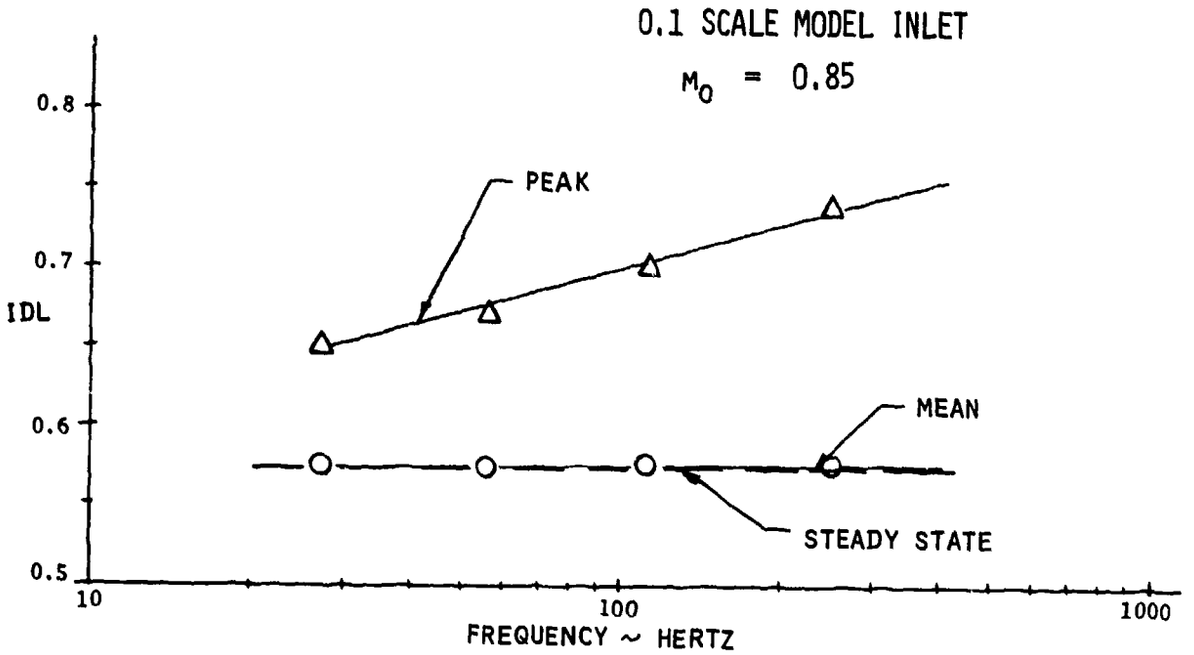

Figure 17 Influence of Frequency on Stall Margin Index

Figure 18 presents average AIP total-pressure ratios are shown for all part-numbers analyzed. These total pressures are the mean values of R1 over the valid flow period as described earlier. With the exception of the M_o = 0.70 and M_c = 0.85 for shock-tube number 1 the mean pressure ratios were quite uniform. The one set of data for two values of W1R at M_o = 0.85 show no weight-flow dependence of the AIP total pressure behind the incident shock. Therefore, the selection of driver total pressures to generate the shock wave appear to give consistent overpressures. Hence, the distortion data for the various shock tubes should also be consistent and may be compared with validity.

The values of IDL for the various Mach numbers tested are given in Figures 19(a) through 19(d). The pre-blast mean IDL, peak IDL, and average IDL are given for each inlet as a function of W1R or yaw angles. The period of valid flow over which these values were selected was described earlier in this report.

The M_o = 0.55 data (Figure 19(a)) have no IDL values in excess of 1.0, while the remaining Mach number data have peak values indicating that the inlet stall-margin allotment has been used. The M_o = 0.70 data (Figure 19(b)) indicate that the yaw angle has little effect upon the inboard inlet pre-blast IDL, while the outboard inlet shows significant increases in IDL with positive yaw angles. The inboard inlet had a peak IDL = 1.2 when the shock originated from shock tube number 3. For the M_c = 0.85 case (Figure 19(c)) the pre-shock and mean IDL's for both inlets show the expected trend of increasing with increasing W1R. However, the outboard inlet peak IDL from Part 608 is the maximum obtained for this Mach number. This may be related to the high AIP total-pressure recovery evident in Figure 18. The inboard inlet peak IDL's behave as would be expected in that they are increasing with increasing W1R. In Figure 19(d), the M_o = 0.90 IDL values are presented. Again the pre-shock IDL's are identical. The outboard inlet showed little change in IDL for the shock tube number 3 firing. The mean AIP total pressures were nearly identical for shock tubes 1 and 3. However, the shock tube 3 data have a less pronounced "N" wave and lower peak pressure than the data from the shock tube 1 firing. The lower IDL for the inboard inlet (see Figure 19(d)) is believed to be a result of the above difference in the total-pressure characteristics.

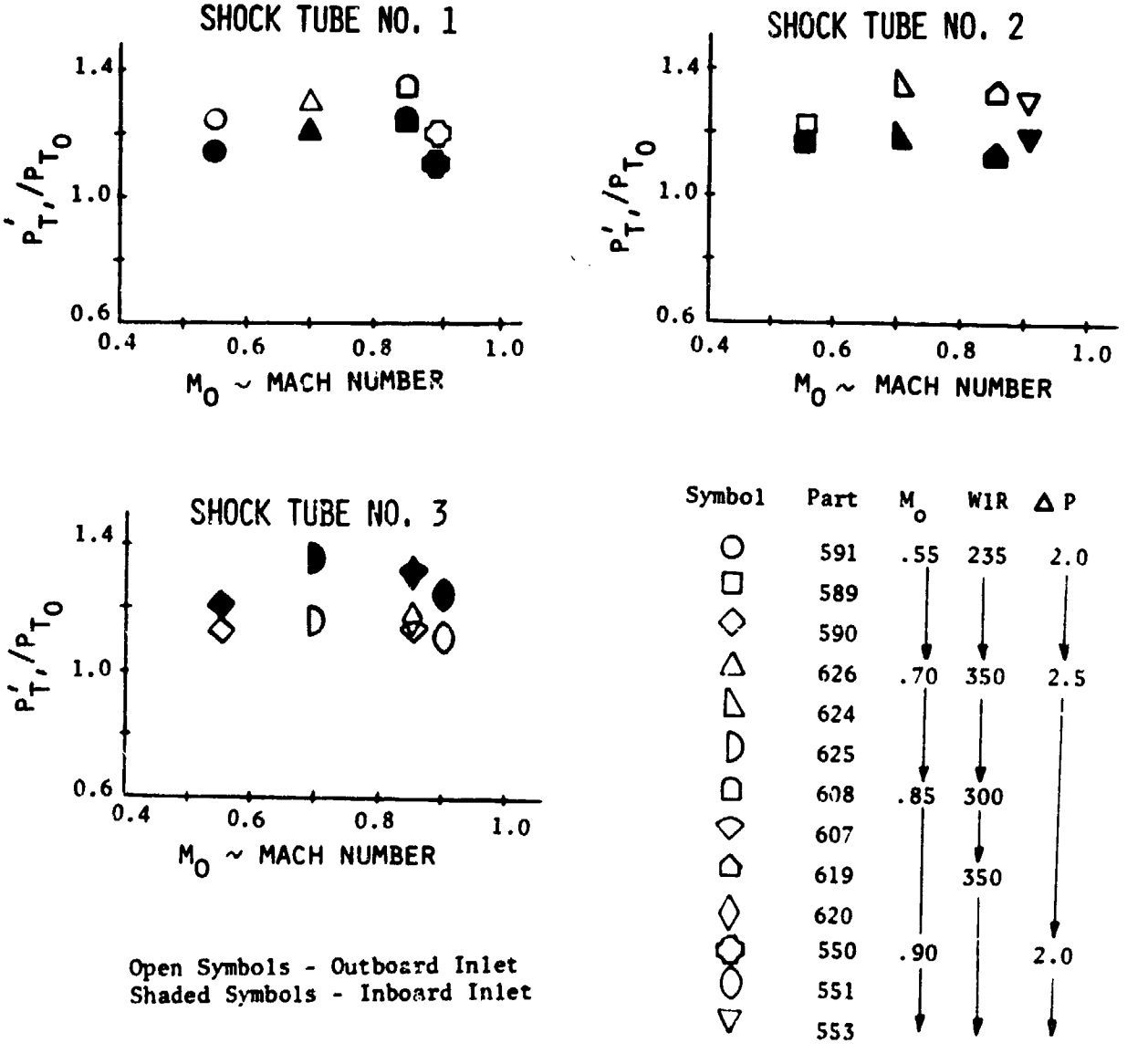

Figure 18 Average AIP Total Pressure Ratio Behind Pressure Disturbance

KAMAN/AEDC DATA

M_0 = 0.85

ψ_0 = 0^0

Symbol	Part	Tube	Target Δ P
○	546	1	2.0
▽	608	1	2.5
□	544	2	2.0
◇	619	2	2.5
△	607	3	2.5
◺	545	3	2.0
D	620	3	2.5

Shaded Symbols are Pre-Shock
Flagged Symbols are Dynamic Peak Values

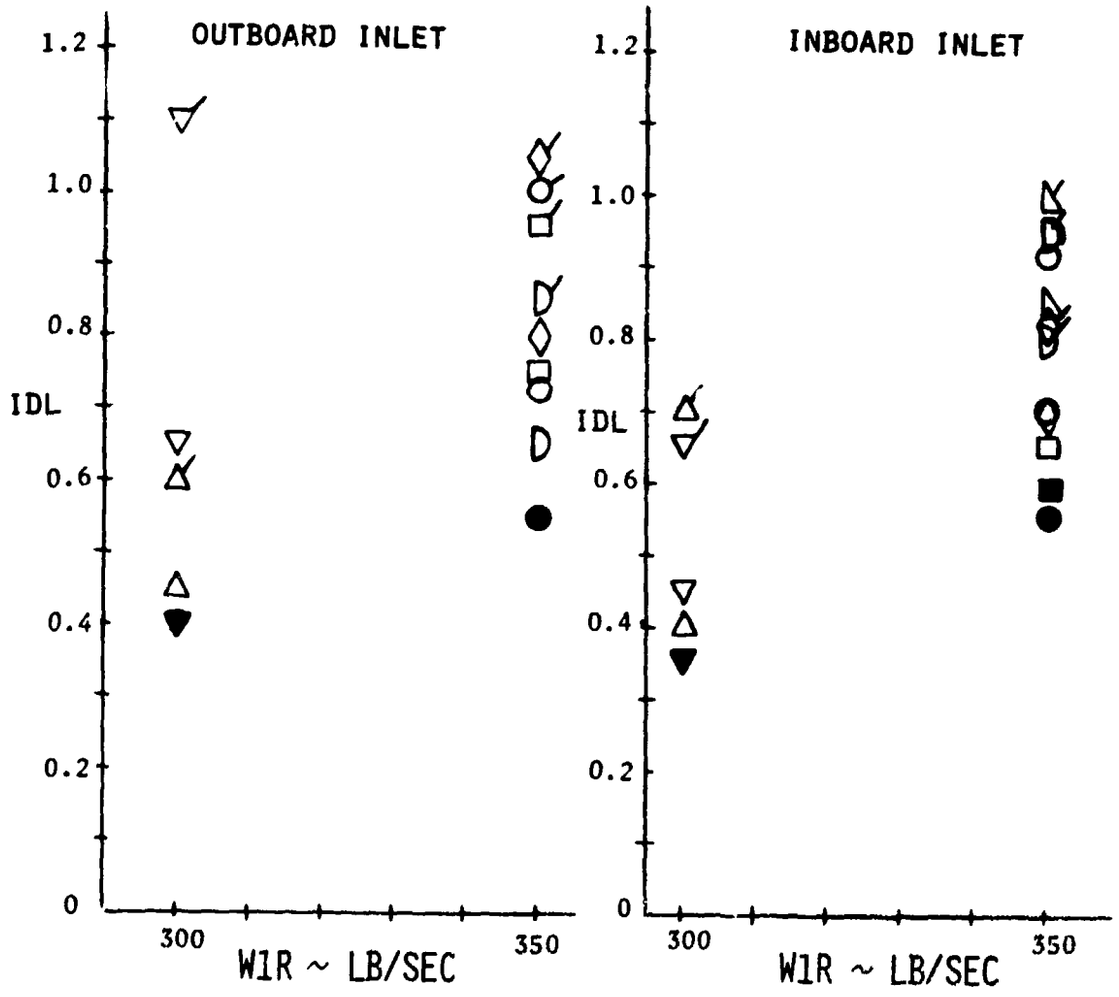

Figure 19(a) Influence of Air Flow on Stall Margin Index

KAMAN/AEDC DATA

M_o = 0.70

WIR = 350 LB/SEC

Symbol	Part	Tube	Target Δ P
○	626	1	2.5
□	624	2	2.5
◇	625	3	2.5
△	570	1	2.0
◺	568	2	2.0
D	569	3	2.0

Shaded Symbols are Pre-Shock
Flagged Symbols are Dynamic Peak Values

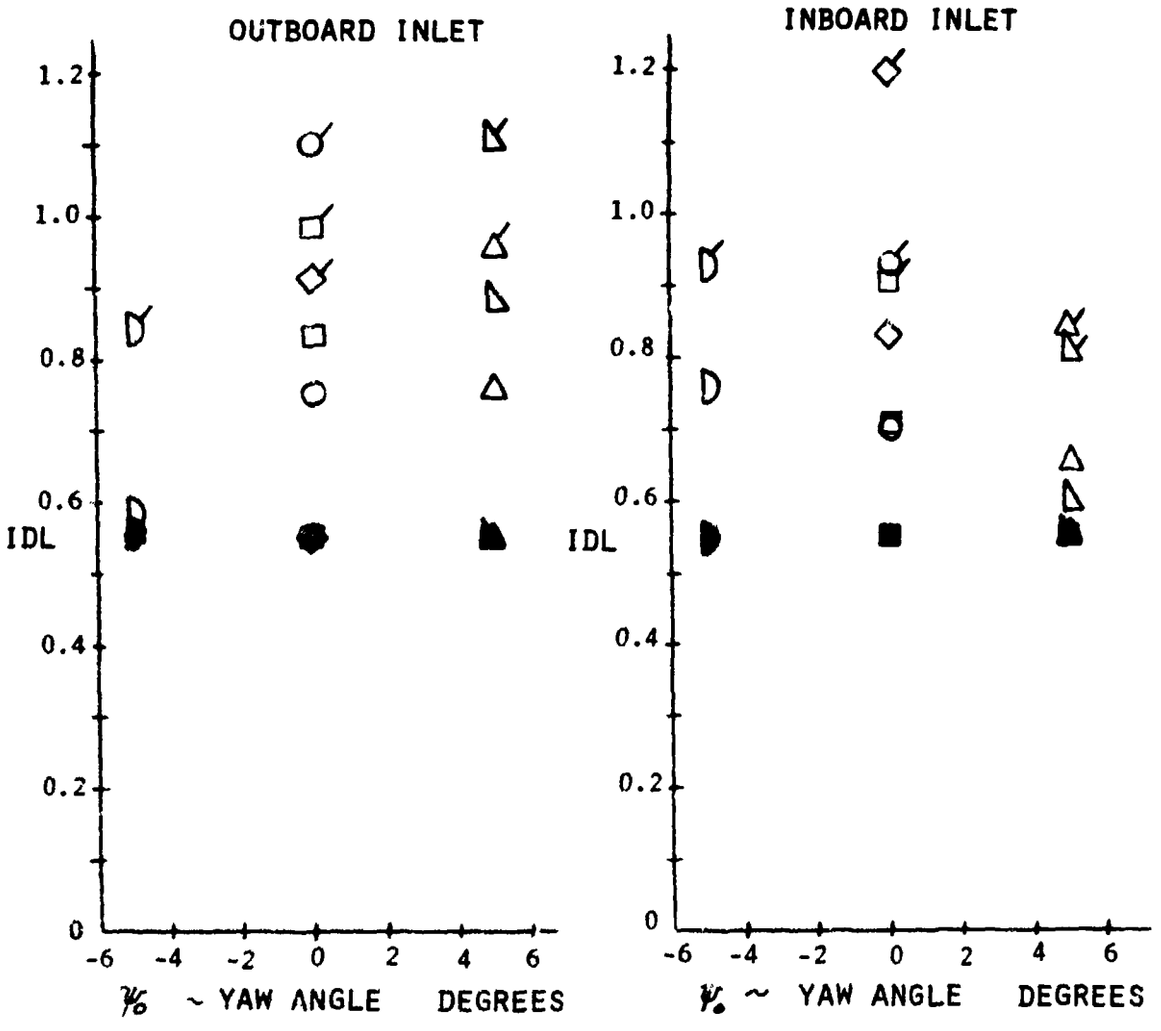

Figure 19(b) Influence of Yaw Angle on Stall Margin Index

SYMBOL	PART	TUBE	TARGET ΔP
▽	608	1	2.5
□	544	2	2.0
◇	619	2	2.5
△	607	3	2.0
◺	545	3	2.0
◗	620	3	2.5

$M_o = 0.85$

$\psi_o = 0^o$

Shaded Symbols are Preblast
Flagged Symbols are Dynamic Peak Values

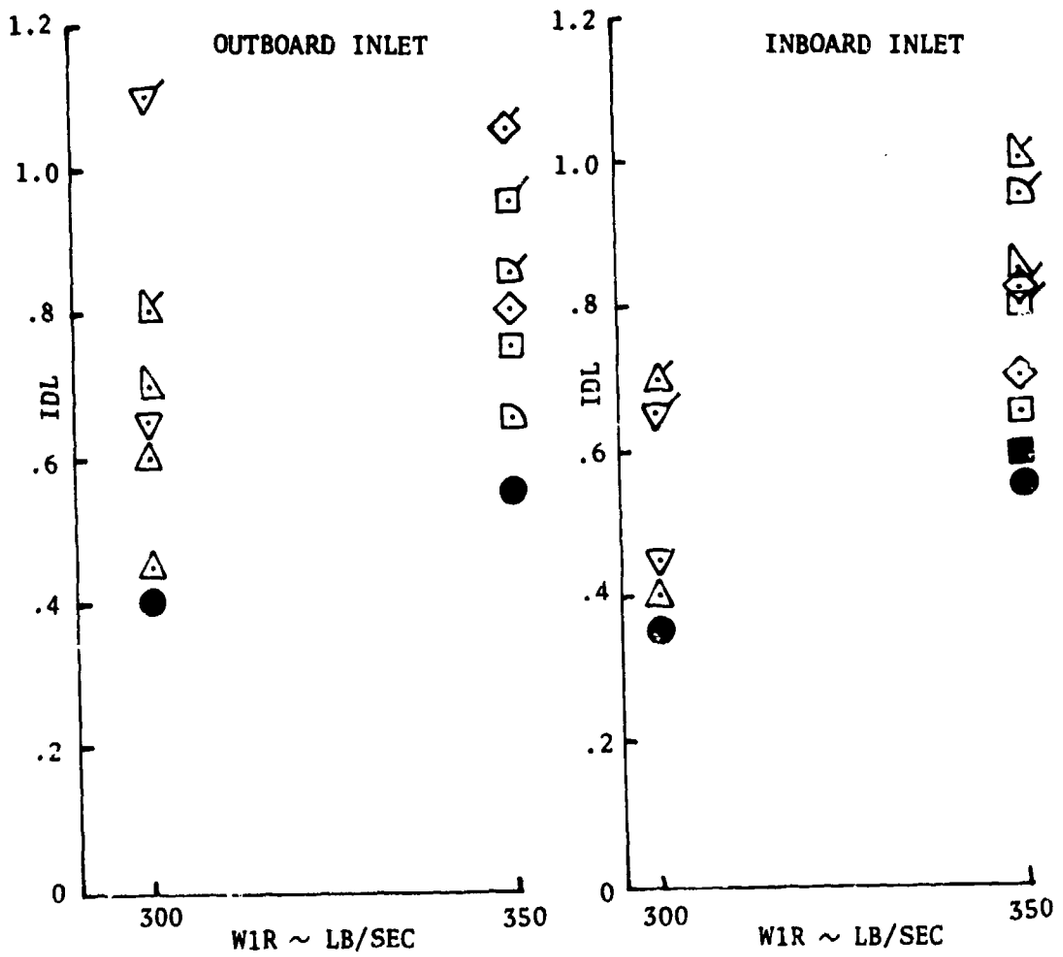

Figure 19(c) Effect of Incident Shock Upon Stall Margin Index

KAMAN/AEDC DATA

$M_0 = 0.90$

$\psi_0 = 0^0$

Symbol	Part	Tube	Target ΔP
○	550	1	2.0
□	553	2	2.0
△	551	3	2.0

Shaded Symbols are Pre-Shock
Flagged Symbols are Dynamic Peak Values

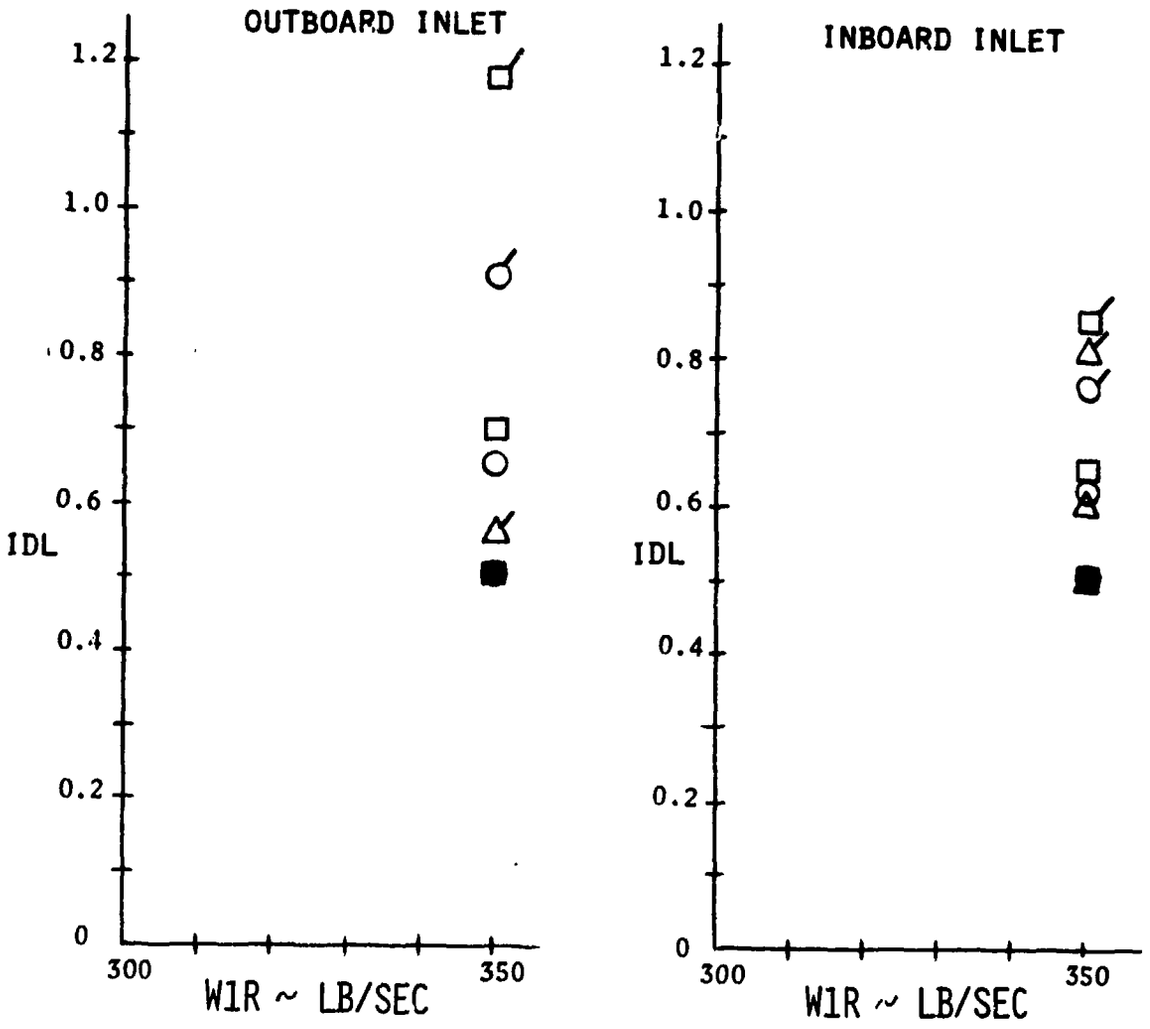

Figure 19(d) Typical Distortion Values @ M = .9

In all of the above cases the windward inlet always showed the maximum activity (IDL), but no general conclusion can be drawn as which shock tube (representing different angles of incidence) generated the maximum IDL's.

As discussed earlier, the data from the Kaman, AEDC tests were not numerically filtered in the computation of the distortion parameters. Thus, the peak IDL values are generally at a frequency much greater than the response of the F101-GE-100. Applying a moving average will reduce the peak IDL to a value closer to the mean IDL's plotted in Figures 19(a) through 19(d). With this in mind, it can be concluded that the Kaman/AEDC pre-blast distortion indices are consistent with previous data and that blast-wave overpressures of the magnitude generated in the present test will not cause engine stall in the B-1 aircraft unless other factors (such as an aircraft maneuver) are simultaneously contributing to the engine/inlet distortion levels.

The distortion data obtained in this test program apply only to the B-1 inlet system or to inlets with close geometric similarity. Application of these distortion data to other inlet systems would be very difficult and should be performed with caution because the shock wave-boundary layer interaction and wave system behavior within the duct would most likely be significantly different and the transmitted wave may not always be planar. Further, a distortion methodology suitable to the engine under consideration would be necessary because Method D referred to herein and used by General Electric and Rockwell may not be applicable.

5.4 COMPARISON WITH FLIGHT TEST DATA

The flight region from M_o = 0.5 to M_o = 1.0 was not predicted to be a region of critical inlet/engine compatibility for the B-1 aircraft. On this basis, very little dynamic data has been reduced, although these data were taken on every flight of aircraft No.'s 1 and 2. The critical compatibility regimes are considered to be take-off and supersonic cruise. However, as was discussed earlier in this report, the DNA test was not intended to be a B-1 inlet/engine program and because of this the specific critical flight regimes of the aircraft were not important to the Kaman/AEDC program. What is of importance to this study is that a relatively small amount of subsonic flight data is available for comparison purposes.

In Figures 20(a) and 20(b) steady-state IDL and WIR, from Reference 24, are given as a function of Mach number for the 500-ft and 20,000-ft altitude cases, respectively. The predicted values of IDL and WIR from wind-tunnel data are also given in these figures. The flight values of IDL are lower than those predicted from the wind-tunnel test program. This result is primarily a result of the higher flight Reynolds number, which gives a thinner inlet boundary layer. This effect is more evident at 500-ft than at 20,000-ft. Also, Figures 20(a) and 20(b) indicate that the flight WIR values are generally considerably lower than those tested in 16T. The lower values of flight WIR will result in lower values of IDL as discussed earlier.

Although extensive dynamic-distortion subsonic-flight test-data reduction has not been performed as noted earlier, one available data set comparing steady-state and dynamic data at $M_o = 0.70$ (from Reference 25) is reproduced in Figures 21(a) and 21(b). Two outboard-engine power settings at Power Lever Angles (PLA) of 16 degrees and 75 degrees, which correspond to idle and maximum dry power, respectively, are presented for zero and -5 yaw angles. At $\psi = 0°$ and PLA = 75° the dynamic IDL is approximately 20 percent greater than the steady-state IDL and for $\psi = -5°$, at the same power setting, dynamic IDL is 36 percent greater. At idle PLA, the $\psi = 0°$ dynamic IDL is 26% greater than the steady-state value and the $\psi = -5°$ dynamic IDL is 56 percent greater than the steady-state value. The shaded areas of the engine face plots in Figures 21(a) and 21(b) represent values in excess of the mean AIP total-pressure ratio (P_T / P_T). The numbers in these plots represent the multipliers of the Δ given in the bullet nose region of each engine-face plot. It should be noted the engine-face pressure distributions are considerably different for the steady-state and peak-dynamic data.

Comparison of the $\psi = 0°$, IDL = 0.598 for flight test (Figure 21(b)) and the mean preblast IDL = 0.55 (peak IDL = 0.73) from Part 626 (shock tube number 1) indicates reasonable agreement. If the data from the present test had been filtered in the same manner as the flight data then the peak IDL would be closer to the mean IDL. The 0.1 scale model Reynolds number is only an order of magnitude lower than the flight Reynolds number, because the wind-tunnel simulated altitude and the flight altitude are close (18,000-ft and 20,000-ft, respectively). The higher

DATA FROM B-1 FLIGHT 1-31

65^{0} WING SWEEP
500 FT. ALTITUDE

FROM: NA-75-300-24

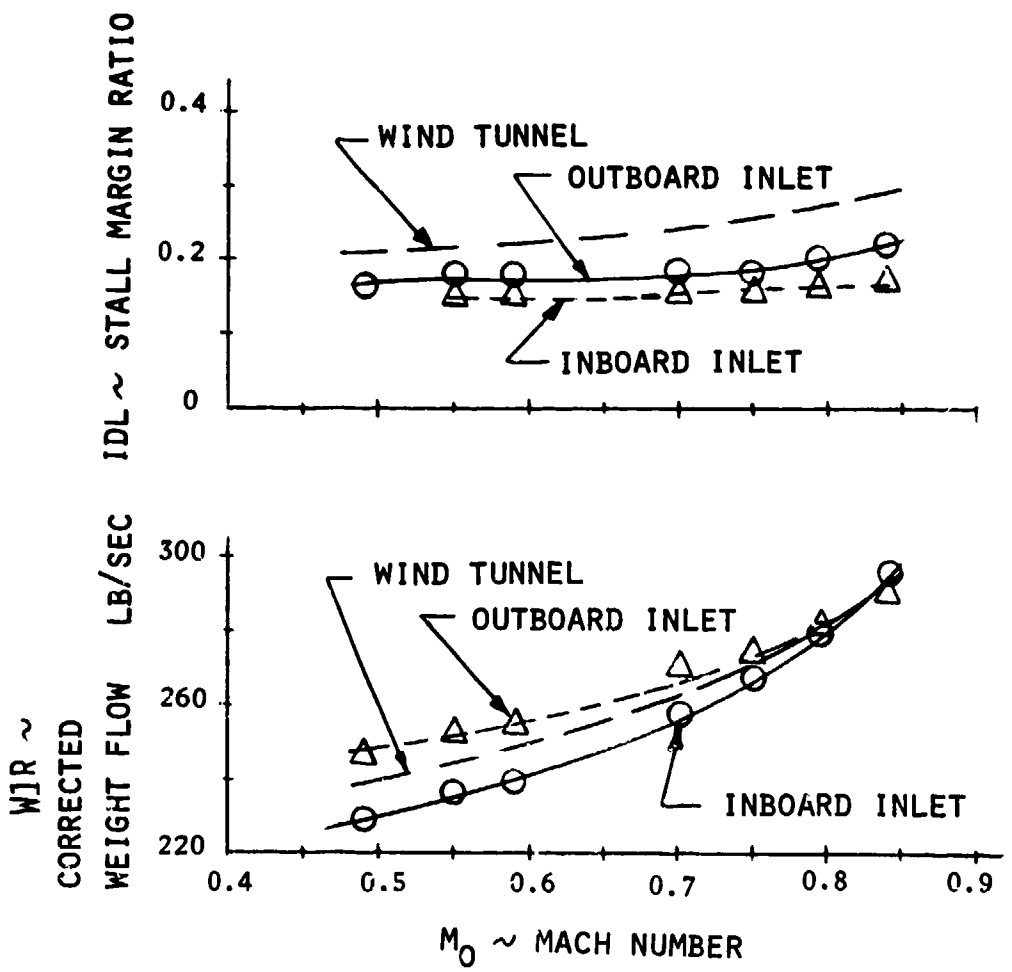

Figure 20(a) Steady-State Inlet Flight Performance

DATA FROM B-1 FLIGHT 1-33
25° WING SWEEP
20,000 FT. ALTITUDE

FROM: NA-75-300-24

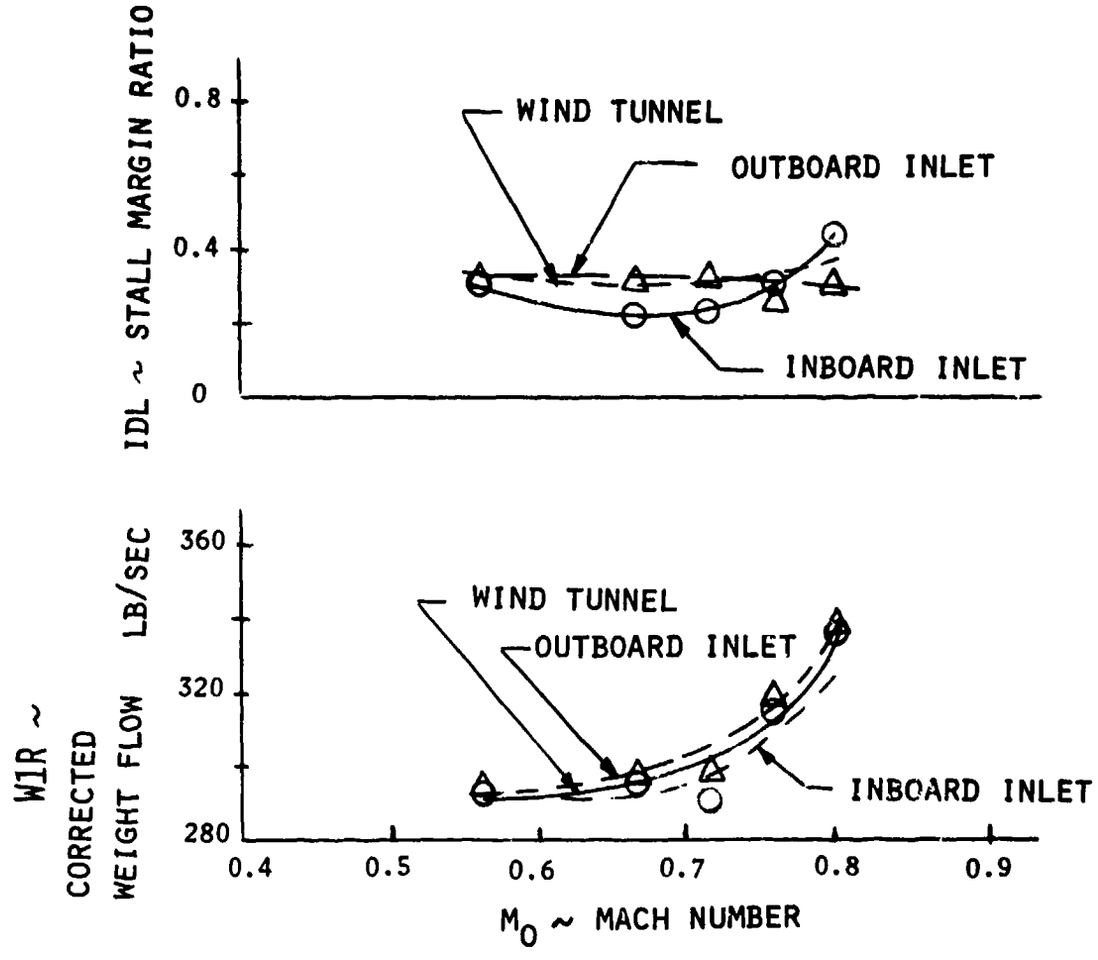

Figure 20(b) Steady-State Inlet Flight Performance

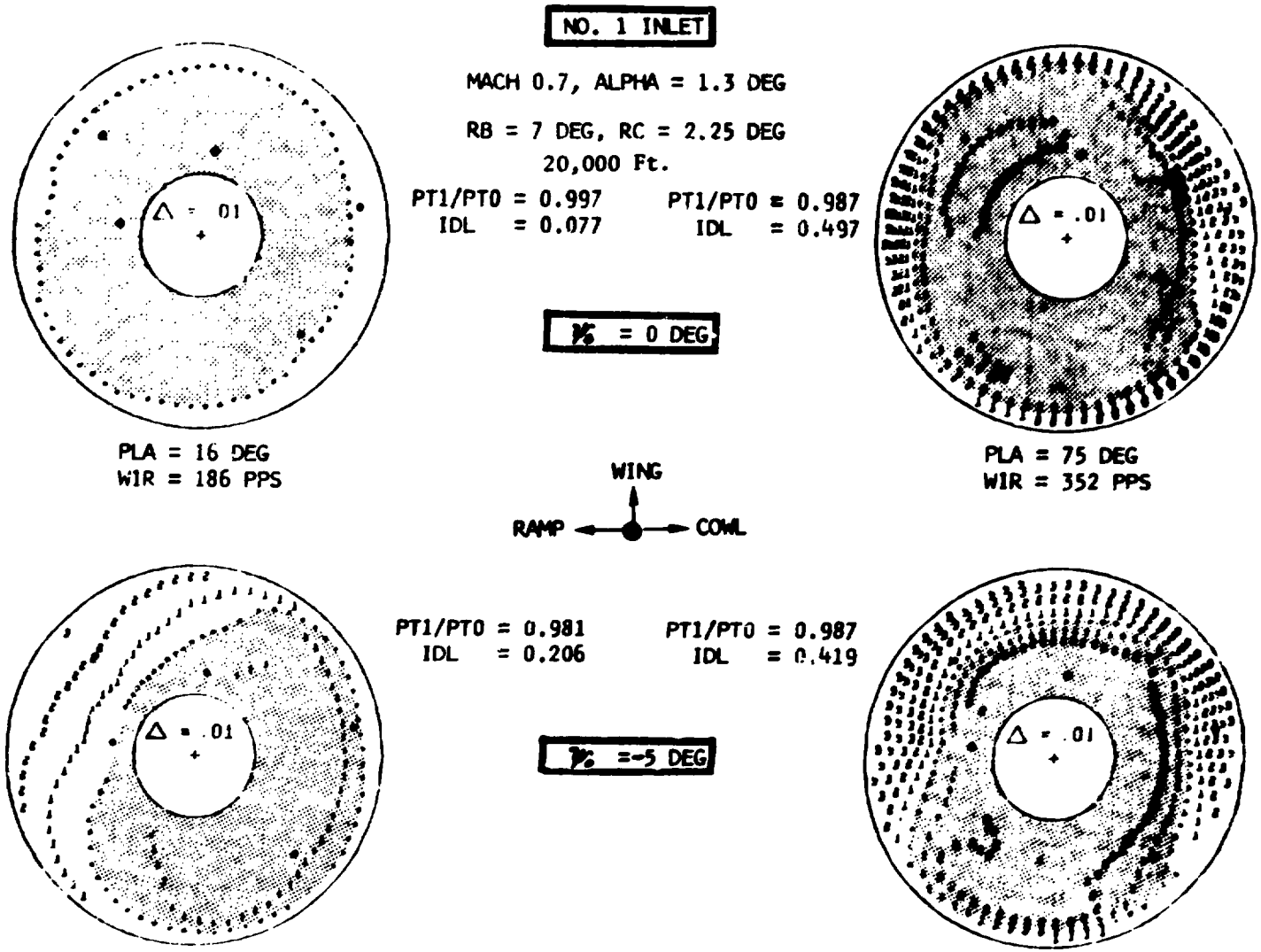

STEADY-STATE TOTAL PRESSURE CONTOURS
From Reference 26

Figure 21(a) Outboard Inlet AIP Steady-State Total Pressure Contours, Mach 0.7, Flight 2-23

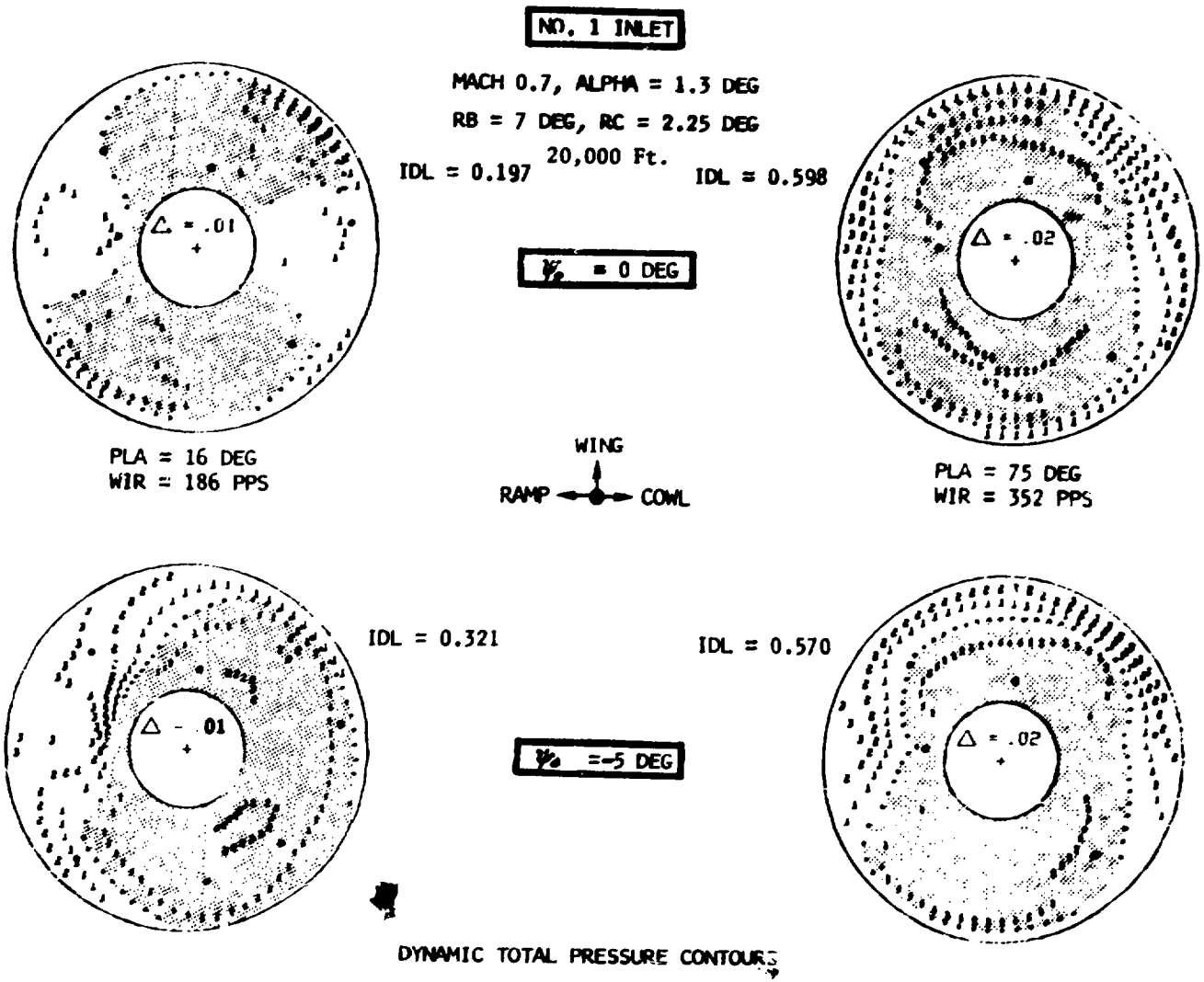

DYNAMIC TOTAL PRESSURE CONTOURS

(MAX IDL SCANS, FILTERED TO 62.5 HZ, SAMPLED AT 360 SPS)

From Reference 26

Figure 21(b) Outboard Inlet AIP Dynamic Total Pressure Contours, Mach 0.7, Flight 2-23

Reynolds number will also decrease the *IDL* as shown in Figure 20(a). It is thus concluded that the blast-wave dynamic-distortion data are in good agreement with those from available flight test.

SECTION 6

CONCLUSIONS

The DNA-supported blast-wave test program conducted by Kaman/AEDC in the AEDC 16T wind tunnel was successful in demonstrating an experimental technique that can be used to superimpose simulated blast waves on a high-velocity subsonic flow and that valid inlet flow distortion measurements can be obtained. A uniform flow duration on the order of 1 to 5 milliseconds was obtained at the inlet/engine aerodynamic interface plane of the 0.1-scale model B-1 vehicle. This flow duration was considered to be sufficient to obtain valid distortion parameters for the inlet.

At the greater shock-wave strengths and inlet airflows, the incident shock wave appears to have been diffracted by the inlet into a planar "N" type wave, having a larger valid test interval than observed at the claw probe. In general, the duct static-pressures histories were qualitatively similar to the claw-probe static pressures outside the inlet. The exception to this observation was for the case of Mach number 0.7 for shock tube #1 in which case there appeared to be a significant second compression in the windward inlet, but these data were later determined to be suspect.

On the basis of the inlet stall-margin (IDL) data obtained in this test, it appears that the B-1 aircraft should not have an engine stall problem for the blast wave orientation and overpressures tested provided that other variables are not simultaneously contributing to the inlet/engine distortion level.

It should be emphasized that the present finding for blast-wave induced distortion apply to the B-1, inlet/engine system only. These results could be applied to geometrically similar inlets and engines with similar distorted flow response, but extreme caution should be used in such an extrapolation.

Good agreement was obtained between the present data and previous wind-tunnel and flight-test distortion indices. The distortion is tip concentrated for both the radial and circumferential modes of distortion. This is a result of the planar shock interacting with the inlet boundary layer.

SECTION 7

RECOMMENDATIONS

In future test programs of this type, it would be desirable to employ larger diameter and longer shock-tube drivers and driven tubes in order to increase the duration of valid flow at the AIP. Reduction of the model size would be helpful in this respect, but it would probably be significantly more costly than changing shock-tube size.

If similar experiments are performed in the future, the AIP distortion data should be digitally filtered to give frequency response compatible with the engine under consideration. The present distortion data for the 0.1-scale model were unfiltered with a frequency of 95,675 samples per second. To make these data compatible with the B-1 F101-GE-100 engine the data should be filtered to 625 Hz (62.5 Hz full scale), the maximum disturbance to which the engine will respond.

It is recommended that a methodology be developed to enable one to determine the engine response to a blast wave front that propagates through the engine. Even in the absence of distortion, this front can produce stall, surge, flameout, or engine damage. Presently, no predictive methodology exists to establish the overall engine response to internal blast-wave propagation.

In addition, it would be extremely valuable to obtain further experimental data, using state-of-the-art techniques, in order to have a solid base upon which a predictive methodology scheme could be built.

REFERENCES

1. Ruetenik, J.R. and Smiley, R.F., "Wind Tunnel Shock Tube Simulation and Evaluation of Blast Effects on an Engine Inlet", Kaman Avidyne Rept. No. KA-TR-147, 15 March 1978.
2. Muirhead, J.C., Naylor, R. and Felt, G.D., "The Transmission of Blast Waves Through an ORENDA 8 Engine from Exhaust to Inlet", DRES, Suffield Memorandum No. 89/69, December 1969.
3. Muirhead, J.C., Taylor, R. and Felt, G.D., "The Transmission of Blast Waves Through an ORENDA 8 Engine", Suffield Technical Note No. 219, July 1969.
4. Muirhead, J.C., "A Review of DRES Studies on the Effect of Blast on Gas Turbine Engines", DRES, Suffield Report No. 267, May 1970.
5. A.E. Fuks, "Distortion Induced Engine Instability", AGARD Lecture Series No. 72, October 1974.
6. P.H. Kutshenreuter and J.L. Younghaus, "Near Term Distortion Methodology/Task Force Results", General Electric Report TIS' R7 AEG4').
7. K.E. Koch and R.L. Rees, "Analysis of Pressure Distortion Testing", NASA CR-2766, December 1976.
8. "Pretest Information of the 0.10 Scale B-1 Inlet Development Model II, Nuclear Blast Effects Test in the AEDC 16-Foot Transonic Propulsion Wind Tunnel", Rockwell International, NA-76-595, 25 August 1976.
9. Rockwell Press. Calib.
10. AEDC Report on Tests
11. Smiley, R.F., "Information for Blast Test of the 0.1 Scale B-1 Inlet Development Model II in the AEDC 16T Propulsion Wind Tunnel", Kaman AviDyne, KA TM-104, 17 August 1976.
12. Johnson, R.H., "Inlet Distortion Scaling of Wind Tunnel Model Results", NASA CR-143840, December 1976.
13. Hale, R.W., Ritter, A., and Ordway, D.E., "Evaluation of Experimental Techniques for Simulating Shock-on-Shock Interaction in a Developmental Ground Test Facility", AEDC-TR-67-111, June 1967.

14. Pierce, D., "Simulation of Blast Waves in a Supersonic Wind Tunnel", RAE Tech. Note Aero 2665, January 1960.

15. Merrit, D.L. and Aronson, P.M., "Study of Blast-Bow Wave Interactions in a Wind Tunnel", AIAA Paper No. 65-5, January 25-27, 1965.

16. Merrit, D.L. and Aronson, P.M., "Wind Tunnel Simulation of Head-On Bow Wave-Blast Wave Interactions", Navy Ord. Lab. Tech. Rept. 67-123, Aug. 9, 1967.

17. Baltakis, F.P., "Shock Interaction Surface Pressures for Hemispherical and Conical Bodies", Navy Ord. Lab. NOLTR-71-27, Feb. 16, 1971.

18. Mason, R.P., "An Experimental Investigation of the Effects of a Blast Wave on a Vehicle in a Supersonic Flow", Cornell Aeronautical Laboratory Rept. CAL No. GM-2673-D-4, October 1969.

19. Dini, D., DiGiorgio, A. and Cardia, S., "Gas Turbine Transient Operating Conditions Due to an External Blast Wave Impulse", AGARD Conference Proceedings No. 177 on Unsteady Phenomena in Turbomachinery, September 1975.

20. Schulze, W.M., Ashby, G.C. and Erwin, J.R., "Several Combination Probes for Surveying Static and Total Pressure and Flow Direction", NACA TN2830, November 1952.

21. Letter from R.J. Christenson, ARO, Inc. to M. Dunn, Calspan dated August 8, 1977.

22. Rudinger, G., "Wave Diagrams for Nonsteady Flow in Ducts", D. Van Nostrand, Inc., New York , 1955

23. McMiller, C.J. and Hurley, O.D. III, "B-1 Inlet Distortion Characteristics at NR/GE Audit Gate #1, Los Angeles Division, North American Rockwell, NA-71-911, June 1971.

24. "Flight Test Progress Report for the B-1 Aircraft", Report No. 24, NA-74-300-24, August 1976.

25. "Flight Test Progress Report for the B-1 Aircraft", Report No. 35, NA-74-300-35, July 1977.

DISTRIBUTION LIST

DEPARTMENT OF DEFENSE

Assistant to the Secretary of Defense
Atomic Energy
ATTN: Executive Assistant

Defense Documentation Center
12 cy ATTN: DD

Defense Nuclear Agency
ATTN: SPAS
ATTN: DDST
ATTN: STSP
4 cy ATTN: TITL

Field Command
Defense Nuclear Agency
ATTN: FCPR

Livermore Division, Fld. Command, DNA
Lawrence Livermore Laboratory
ATTN: FCPRL

NATO School (SHAPE)
ATTN: U.S. Documents Officer

Under Secy. of Def. for Rsch. & Engrg.
ATTN: Strategic & Space Systems (OS)
ATTN: Offensive Systems, M. Atkins

DEPARTMENT OF ARMY

Harry Diamond Laboratories
Department of the Army
ATTN: DELHD-N-NP
ATTN: DELHD-N-P, J. Gwaltney

U.S. Army Ballistic Research Labs.
ATTN: DRXBR-BLT, W. Taylor

U.S. Army Materiel Dev. & Readiness Cmd.
ATTN: DRCDE-D, L. Flynn

U.S. Army Nuclear & Chemical Agency
ATTN: Library

DEPARTMENT OF THE NAVY

Naval Material Command
ATTN: MAT 08T-22

Naval Research Laboratory
ATTN: Code 2627

Naval Weapons Evaluation Facility
ATTN: L. Oliver

Office of Naval Research
ATTN: Code 465

Strategic Systems Project Office
ATTN: NSP-272

Naval Surface Weapons Center
White Oak Laboratory
ATTN: K. Caudle

DEPARTMENT OF THE AIR FORCE

Aeronautical Systems Division, AFSC
ATTN: ENFT, R. Bachman
4 cy ATTN: ENFTV, D. Ward

Air Force Aero-Propulsion Laboratory, AFSC
ATTN: TBC, M. Stibich

Air Force Materials Laboratory, AFSC
ATTN: MBE, G. Schmitt

Air Force Weapons Laboratory, AFSC
ATTN: DYV, A. Sharp
ATTN: DYV, G. Campbell
ATTN: SUL

Foreign Technology Division, AFSC
ATTN: SDBF, S. Spring

Strategic Air Command
Department of the Air Force
ATTN: XPFS, B. Stephan

DEPARTMENT OF DEFENSE CONTRACTORS

Aerospace Corp.
ATTN: W. Barry

Avco Research & Systems Group
ATTN: J. Patrick
ATTN: P. Grady

Boeing Co.
ATTN: R. Dyrdahl
ATTN: S. Strack
ATTN: E. York

Boeing Wichita Co.
ATTN: R. Syring

Calspan Corp.
ATTN: M. Dunn
ATTN: A. Davis

Effects Technology, Inc.
ATTN: E. Bick
ATTN: R. Parisse
ATTN: R. Wengler

General Dynamics Corp.
ATTN: R. Shemensky

General Electric Co.-TEMPO
Center for Advanced Studies
ATTN: DASIAC

General Research Corp.
ATTN: T. Stathacopoulos

Kaman AviDyne
Division of Kaman Sciences Corp.
ATTN: N. Hobbs
ATTN: R. Ruetenik
ATTN: E. Criscione

DEPARTMENT OF DEFENSE CONTRACTORS (Continued)

Kaman Sciences Corp.
ATTN: D. Sachs

Los Alamos Technical Associates, Inc.
ATTN: P. Hughes

McDonnell Douglas Corp.
ATTN: J. McGrew

Prototype Development Associates, Inc.
ATTN: C. Thacker
ATTN: J. McDonald

R & D Associates
ATTN: C. MacDonald
ATTN: J. Carpenter
ATTN: F. Field
ATTN: A. Kuhl

DEPARTMENT OF DEFENSE CONTRACTORS (Continued)

Rockwell International Corp.
ATTN: R. Sparling
ATTN: R. Mosnan

Sandia Laboratories
ATTN: Doc. Con. for A. Lieber

Science Applications, Inc.
ATTN: D. Hove

Science Applications, Inc.
ATTN: J. Dishon

SRI International
ATTN: G. Abrahamson